J. Fluid Mech. (1999), *vol.* 388, *pp.* 69–113. Printed in the United Kingdom

Nonlinear capillary wave distortion and disintegration of thin planar liquid sheets

By C. MEHRING AND W. A. SIRIGNANO

Department of Mechanical and Aerospace Engineering, University of California, Irvine, CA 92697, USA

(Received 27 April 1998 and in revised form 19 October 1998)

Linear and nonlinear dilational and sinuous capillary waves on thin inviscid infinite and semi-infinite planar liquid sheets in a void are analysed in a unified manner by means of a method that reduces the two-dimensional unsteady problem to a one-dimensional unsteady problem. For nonlinear dilational waves on infinite sheets, the accuracy of the numerical solutions is verified by comparing with an analytical solution. The nonlinear dilational wave maintains a reciprocal relationship between wavelength and wave speed modified from the linear theory prediction by a dependence of the product of wavelength and wave speed on the wave amplitude. For the general dilational case, nonlinear numerical simulations show that the sheet is unstable to superimposed subharmonic disturbances on the infinite sheet. Agreement for both sinuous and dilational waves is demonstrated for the infinite case between nonlinear simulations using the reduced one-dimensional approach, and nonlinear two-dimensional simulations using a discrete-vortex method. For semi-infinite dilational and sinuous distorting sheets that are periodically forced at the nozzle exit, linear and nonlinear analyses predict the appearance of two constant-amplitude waves of nearly equal wavelengths, resulting in a sheet disturbance characterized by a long-wavelength envelope of a short-wavelength oscillation. For semi-infinite sheets with sinuous waves, qualitative agreement between the dimensionally reduced analysis and experimental results is found. For example, a half-wave thinning and a sawtooth wave shape is found for the nonlinear sinuous mode. For the semi-infinite dilational case, a critical frequency-dependent Weber number is found below which one component of the disturbances decays with downstream distance. For the semi-infinite sinuous case, a critical Weber number equal to 2 is found; below this value, only one characteristic is emitted in the positive time direction from the nozzle exit.

1. Introduction

The instability and breakup of free liquid sheets are of considerable scientific and technological importance, and have been extensively studied in connection with atomization, spray combustion (Dombrowski & Munday 1968; Lefebvre 1989) and curtain coating (Brown 1961). The dynamics of thin sheets of fluid was studied as long as one and a half centuries ago by Savart (1833), Boussinesq (1869*a*, *b*), Bond (1935), Dorman (1952), Fraser & Eisenklam (1953) and Dombrowski & Fraser (1954).

This section of the paper focuses on a review of the literature on the analyses of capillary wave motion on planar liquid sheets.

1.1. *Linear two-dimensional planar sheets*

Theoretical investigations on the linear stability of (thin) planar liquid sheets in a surrounding gas flow were first conducted by York, Stubbs & Tek (1953) and Squire (1953) and later by Hagerty & Shea (1955). Hagerty & Shea (1955) could show that by linear analysis, only two modes of sheet deformation are possible on planar sheets, i.e. sinuous (antisymmetric) waves and dilational (symmetric) or 'sausage' mode waves. Hagerty & Shea were also the first to compare their theoretical results with planar sheet experiments with and without modulation of the sheets at the nozzle exit. The linear analyses presented by Squire (1953) and Hagerty & Shea (1955) were generalized later by Dombrowski & Hooper (1962) and Rangel & Sirignano (1991), the latter extending the linear analysis for the complete range of liquid-to-gas density and thickness-to-disturbance wavelength ratios.

Theoretical analyses on the dispersive nature of linear capillary waves on (thin) planar sheets were first provided by Taylor (1959*a*); for thin sheets, i.e. sheets with disturbance wavelengths significantly larger than the sheet thickness, linear dilational (capillary) waves are dispersive, whereas linear sinuous (capillary) waves are non-dispersive. Similar observations were made later by Lin & Roberts (1981), Mehring, Kim & Sirignano (1997) and Mehring & Sirignano (1998*a*), the latter two by using a simplified one-dimensional theory based on the assumption of thin sheets.

The predominant appearance of the sinuous or dilational mode of sheet distortion was discussed by Fraser *et al.* (1962) and continued by Dombrowski & Hooper (1962) in their analysis of the effect of ambient density on the sheet-breakup mode. Dombrowski & Hooper (1962) made the observation that, at atmospheric density, sheet breakup occurs through sinuous waves, whereas at higher densities, both sinuous and dilational modes appear to be present, the latter being dominant at very high density ratios. This phenomenon has also been observed later theoretically and experimentally by Li & Tankin (1991), Rangel & Sirignano (1991) and Mansour & Chigier (1991).

Squire (1953) and later Taylor (1959*b*) observed that the linear stability analysis of a liquid sheet moving in an ambient gas is not able to predict sheet breakup but merely wave amplification of small sinuous disturbances. Following this observation, Taylor (1959*b*) presented a simple analysis for the dynamics of a free edge bounding a sheet of uniform thickness. He used this simplified theory to predict the breakup length of a conical liquid sheet which had also been investigated experimentally. Based on the mean wavelength of the sheet-thickness variations caused by oscillations within the atomizer, Taylor also proposed a diameter for the droplets generated by the disintegrating sheet. Drop-size predictions for aerodynamically induced fan sheet disintegration were obtained by Fraser *et al.* (1962) and Dombrowski & Hooper (1962) by considering that the most rapidly growing wave (predicted according to Squire 1953 or Hagerty & Shea 1955) is detached at the leading edge in the form of a ribbon half a wavelength wide. This ribbon forms a ligament which subsequently disintegrates according to Rayleigh's capillary instability analysis. Taylor's 'edge-dynamics' theory has also been employed by other authors (Brown 1961; Antoniades, Godwin & Lin 1980) to predict the breakup length of liquid curtains.

The spatial stability of planar sheets was first considered by Lin (1981), who provided a linear stability analysis for thin viscous two-dimensional liquid sheets in a void and under the influence of gravity. The latter is of importance in connection with a process called curtain coating where a two-dimensional liquid sheet, guided by two wires, falls onto a moving substrate to provide a uniform coating (Brown 1961). The (thin) liquid curtain is temporally and spatially stable for varicose disturbances and

temporally stable for sinuous disturbances. As reported, only the spatially growing (sinuous) disturbances with negative group velocity were unstable, in agreement with the experimental results by Brown (1961). Lin, Lian & Creighton (1990) analysed the curtain problem, with the influence of the ambient gas considered. Absolute and convective stability (to be defined later) of the sheet were determined from the corresponding characteristic equations for complex wavenumbers and frequencies according to Briggs (1964) and Bers (1983). (See also Li 1993 in this context.) Lin *et al.* (1990) found that the sheet is convectively unstable for both sinuous and dilational modes. However, the instability with respect to sinuous disturbances at Weber numbers (here defined as the ratio of inertia force to surface tension force per unit area of the gas–liquid interface) $We < 2$ as observed experimentally by Brown (1961) and predicted theoretically for the case of a viscous curtain in a void by Lin (1981) was not observed in the same way as by the latter author. Lin *et al.* (1990) explain this instability through the presence of a 'pinch-point' singularity at zero wavelength and zero wavenumber.

In recent years, Li (1993) presented a linear analysis (related to the study by Lin *et al.* 1990) on the spatial stability of a thin two-dimensional viscous liquid sheet in an inviscid gas medium similar to the temporal analysis presented by Li & Tankin (1991). Spatial and temporal instabilities were found to differ quantitatively and qualitatively at low Weber numbers, but give almost identical results at large Weber numbers (Li 1994).

Linear analyses of modulated semi-infinite two-dimensional sheets exiting from a nozzle or atomizer were only considered within the work by Mehring & Sirignano (1997, 1998*b*) for the case of a zero-density ambient gas. Prior to this work, capillary waves on planar liquqid sheets emanating from a nozzle or atomizer had already been observed and investigated experimentally by Hashimoto & Suzuki (1991) and held responsible by Clark & Dombrowski (1972) for the observed discrepancy between their theoretical (infinite sheet) and experimental results for fan sheets.

Sheet attenuation, i.e. the variation of sheet thickness with distance in diverging nozzle configurations such as fan spray nozzles, had been considered by Taylor (1959*b*), and later by Dombrowski, Hasson & Ward (1960). Their results were subsequently used by Dombrowski & Johns (1963) in a linear stability analysis of attenuating (thinning in the flow direction) sheets, and by several other authors for the prediction of drop sizes from fan sheets as described above (Fraser *et al.* 1962; Dombrowski & Hooper 1962; Weihs 1978).

The effects of liquid (and gas) viscosity were analysed by several of the previously mentioned authors and others: Dombrowski & Johns (1963), Crapper, Dombrowski & Jepson (1975), Lin (1981), Lin & Roberts (1981), Lin *et al.* (1990) and Ramos (1996). Lin (1981) showed that liquid viscosity has the dual roles of increasing the amplification rate as well as damping the growth rate of sinuous sheet disturbances, a result that was also observed later by Li & Tankin (1991) and Li (1993).

In the context of comparisons between experimental results and predictions made by linear theory, the importance of nozzle vibrations was considered, discussed and/or demonstrated by Taylor (1959*b*), Crapper, Dombrowski & Pyott (1975*a*) and Crapper & Dombrowski (1984).

Planar liquid sheets were also analysed as limiting cases of annular sheet configurations (Crapper, Dombrowski & Pyott 1975*b*; Meyer & Weihs 1987; Shen & Li 1996) recovering the results of previously mentioned authors (Squire 1953; Li & Tankin 1991).

In the past decades, there have been several interesting articles that discuss spatially

developing hydrodynamic instabilities and categorize the instabilities as either absolute or convective. See, for example, Bers (1983) and Huerre & Monkewitz (1990). This categorization depends upon the temporal response to a disturbance at the very location of the disturbance. When the initial disturbance results in a local growth of the disturbance over a long time according to linearized theory, then the phenomenon is classified as an absolute instability. On the other hand, when the initial disturbance results in a growing disturbance that propagates away from the original location leaving only temporal decay at the original location, it is classified as a convective instability. Of course, no growth of any kind of the original disturbance indicates a stable phenomenon. Our analysis will relate to disturbances that do not grow in amplitude so the categorization in its original form is not useful here. The analysis presented here (similar to the analysis by Lin 1981 mentioned before) will consider local spatial theory in the strict sense (real frequency and complex wavenumber) in order to investigate the linear behaviour of modulated semi-infinitely long sheets and temporal theory (real wavenumber and complex frequency) in order to study periodically disturbed infinite sheets. The former theory considers spatial disturbances originating from a time-dependent locally-imposed finite disturbance (previously referred to as spatial stability analysis) and the latter theory treats the temporal evolution of periodic disturbances due to an initial deviation from the undisturbed flow condition (previously identified as temporal stability analysis).

1.2. *Nonlinear two-dimensional planar sheet analyses*

As noted earlier, linear stability analyses of planar sheets do not predict sheet breakup due to sinuous disturbances, the latter being dominant at low gas-to-liquid density ratios (Rangel & Sirignano 1991; Mansour & Chigier 1991).

Clark & Dombrowski (1972) considered a second-order (temporal) analysis of the aerodynamic growth of sinuous waves on parallel-sided, i.e. non-attenuating, inviscid sheets. They predicted the appearance of the first-harmonic dilational mode due to energy transfer from the fundamental sinuous mode, which provided sheet breakup at half-wavelengths of the fundamental mode and at locations close to the maximum deflection region of the sheet. A similar observation was made in the nonlinear sheet analyses by Rangel & Sirignano (1991) using a discrete-vortex method for the analysis of a planar liquid sheet in a gas of non-zero density. Jazayeri & Li (1996) used a third-order stability analysis for an inviscid periodically disturbed liquid sheet moving in an inviscid (and incompressible) gas stream and also concluded that the sheet ruptures at half-wavelengths of the fundamental sinuous mode. However, the sheet distortion predicted by Jazayeri & Li (1996) is greatly influenced by the first and second harmonics of the sinuous mode. In agreement with Rangel & Sirignano (1991), Jazayeri & Li (1996) observed that the nonlinear growth rates for the sinuous mode are less than suggested by the linear prediction.

After Clark & Dombrowski (1972) developed their nonlinear (temporal) analysis based on experimental observations from fan sheet experiments, nonlinear effects were also studied by Crapper *et al.* (1975*a*) for the spatial stability of thin liquid sheets forced at the nozzle exit. Based on experimental observations, Crapper *et al.* (1975*a*) developed a 'preliminary' large-amplitude theory considering the formation of vortices in the gas flow surrounding the liquid stream. Asare, Takahashi & Hoffman (1981) also investigated the stability of liquid sheets (at two thicknesses and at variable air pressures) harmonically forced at the nozzle (sinuous disturbances only). Deviations between experimental observations and linear theory were found for higher forcing frequencies and at larger downstream positions where the wave-envelope amplitude

appeared to saturate before sheet breakup. Similar observations were made by Crapper *et al.* (1975*a*). Asare *et al.* (1981) also provided a simplified trajectory theory based on the linearized force balance for a fluid particle in the crest of a propagating wave.

Nonlinear (capillary) waves on fluid sheets in a void were studied by Kinnersley (1976) whose analysis was a generalization of Crapper's (1957) exact solution for a fluid of infinite depth. The former analysis was later revised and extended by Hogan (1986). Sheet breakup at half-wavelengths for sinuous waves and at points interspaced by one wavelength for dilational distorting sheets was observed by Dombrowski & Hooper (1962).

Weakly nonlinear analyses for capillary dilational waves on planar sheets by Matsuuchi (1974, 1976) revealed that two periodic (dilational) wave trains of finite amplitude and with different wavelengths are 'modulationally' unstable and lead to sheet breakup even without the interaction with an ambient gas. This is in contrast to corresponding linear analyses and the observation made by Dombrowski & Hooper (1962), i.e. that a flat laminar sheet injected *in vacuo* is stable. The same observation as described by Matsuuchi (1976) is also made within the present analysis. The recent work and the work presented by Mehring & Sirignano (1998*a*) extend the Matsuuchi analysis to general (i.e. dilational and sinuous) capillary waves on planar sheets. For sinuous waves, the same characteristic nonlinear behaviour was observed as previously described by Rangel & Sirignano (1991) for aerodynamically forced liquid sheets, including the nonlinear transverse oscillation of initially linear (sinuous) travelling waves. In their analysis of the dilational mode only, Mehring *et al.* (1997) also observed a temporal steepening and desteepening of initially linear dilational travelling waves with sheet breakup at points interspaced by one wavelength.

Nonlinear analyses of planar sheets in a void and with harmonic forcing at the nozzle exit were analysed only by Meier, Klöpper & Grabitz (1992) and Mehring & Sirignano (1997, 1998*b*). The latter observed that, as in their linear analysis of the corresponding sheet configuration, the (sinuous and dilational) sheet distortion is in general characterized by a long-wavelength envelope of a short-wavelength oscillation. (See also Hashimoto & Suzuki 1991.) Fluid agglomeration in the maximum deflection region of the sheet found on transversely modulated sheets was similar to that in the corresponding infinite case of sinuous travelling waves. Also, for sheets with dilational forcing at the nozzle exit, fluid was found to accumulate into fluid lumps, with increased sheet thinning and breakup at points close to these blobs of fluid. The analysis presented by Meier *et al.* (1992) focused on the dilational mode of sheet modulation and did not consider surface tension; therefore, the physics, especially in the thin sheet limit, can be shown to be profoundly different from the application of interest.

1.3. *Three-dimensional planar sheets*

Only a few three-dimensional or quasi-three-dimensional analyses on planar liquid sheets have been reported so far in the literature. Arai & Hashimoto (1985) presented experimental results on the three-dimensional breakdown of a planar liquid sheet in a high-speed cocurrent uniform gas stream; more extensive anlayses of a similar configuration were later conducted by Mansour & Chigier (1990, 1991). Within their work, Arai & Hashimoto (1985) also presented a perturbation analysis of the corresponding inviscid three-dimensional boundary value problem. Ibrahim & Akpan (1996) presented a three-dimensional linear analysis of a periodically disturbed planar viscous liquid sheet in an inviscid gas medium. Preliminary results on the nonlinear distortion of a thin planar inviscid liquid sheet in a void and with three-dimensional disturbances were recently presented by Kim & Sirignano (1997, 1998) for infinite

periodically disturbed and semi-infinite modulated sheets (dilational disturbances only). Their nonlinear analyses are based on the analyses presented by Sirignano & Mehring (1996), Mehring *et al.* (1997) and Mehring & Sirignano (1997, 1998*a*, *b*) using a reduced-dimension approach to describe the nonlinear distortion of thin planar two-dimensional liquid sheets.

The analysis of the stability or distortion of thin sheets of liquid of arbitrary shape in terms of a reduced-dimension analysis, i.e. a one- or two-dimensional continua theory, has also been proposed by Entov (1982). Although general dynamic equations were derived including the effects of complex rheology of the liquid sheets considered, only stationary motions and small perturbations of the film about its stationary position were considered. More recent work on this topic was presented by Zak (1979) and Yarin (1993), the latter including a detailed review of previous work on liquid sheet rheology and hydrodynamics.

A numerical analysis of free liquid sheets by using a 'general-purpose' multi-fluid method has been reported only by Poo & Ashgriz (1988). Although similar techniques such as VOF (volume-of-fluid) methods (e.g. Kothe *et al.* 1996), level-set methods (e.g. Sussman *et al.* 1997) or other front-tracking finite-difference techniques (e.g. Nobari & Tryggvason 1996) are also able to predict the nonlinear distortion of liquid sheets, the accuracy of these predominantly Eulerian techniques is difficult to retain at an acceptable level when thin sheets with considerable nonlinear distortion are considered. More accurate results might be expected by Lagrangian methods for interfacial flows (Shyy *et al.* 1996), e.g. boundary-element techniques (Heister 1997) or discrete-vortex methods (Baker, Meiron & Orszag 1982; Rangel & Sirignano 1988, 1991) as well as the prescribed Eulerian techniques if combined with dynamic regridding at the location of the fluid interfaces. However, such simulations are computationally very intensive and do not typically yield the same insights as the analytical considerations described previously.

Many interesting studies have been performed for round liquid jets. Some precede the first studies on liquid sheets and many parallel efforts on the sheet configuration. See the pioneering work of Rayleigh (1879) and the review by Bogy (1978).

1.4. *Present analysis*

The treatment in this paper for nonlinear dilational and sinuous waves follows a system of equations and approach originally determined by the senior author for the limiting case of small sheet thickness compared to wavelength. The first computations for dilational waves were presented by Sirignano & Mehring (1996). This first solution was valid only for short times and did not capture the full nonlinear wave development. Approximate forms of the equations were solved in a manner valid for long times by Mehring *et al.* (1997) and Mehring & Sirignano (1997) for dilational and sinuous waves in both the infinite and semi-infinite configurations (temporal and spatial stability, respectively). In this paper, certain approximations are removed and the various analyses (linear and nonlinear treatments, dilational and sinuous modes, infinite and semi-infinite configurations) are unified. Comparisons with fully two-dimensional computations are also made. After the study was launched and the first publication was printed, the authors discovered the work of Matsuuchi (1974, 1976) that very closely paralleled a portion of this work in the narrow domain of dilational waves on infinite sheets.

In § 2, the reduced-dimension system of equations is formulated; it is derived from the fully two-dimensional problem by using polynominal expansions of the dependent flow variables in terms of $[y - \bar{y}(x,t)]$ where y denotes the direction perpendicular to

the undisturbed sheet or main flow direction and $\overline{y}(x,t)$ is the instantaneous location of the sheet centreline in the y-direction. The temporal stability of infinite sheets is considered in § 3 with both linear and nonlinear analyses for both dilational and sinuous mode waves. An exact nonlinear solution is presented for the dilational case in § 3.2. More general nonlinear solutions are found by finite-difference computations and presented in § 3.3. The spatial stability on a semi-infinite sheet is discussed in § 4 for linear and nonlinear treatments of both wave modes. Conclusions are presented in § 5.

2. Governing equations

A thin incompressible inviscid planar liquid sheet flowing in a void and zero gravity is considered. Here, the specification 'thin' implies that only fluid sheets are considered for which the thickness of the sheet is small compared to the disturbance wavelength. Our derivation below will be an extension of the analysis by Sirignano & Mehring (1996).

The governing equations, describing the unsteady motion within an incompressible inviscid two-dimensional liquid sheet at zero gravity are given by

$$\frac{\partial u}{\partial x} + \frac{\partial v}{\partial y} = 0, \tag{2.1}$$

$$\frac{\partial u}{\partial t} + u\frac{\partial u}{\partial x} + v\frac{\partial u}{\partial y} = -\frac{1}{\rho}\frac{\partial p}{\partial x}, \tag{2.2}$$

$$\frac{\partial v}{\partial t} + u\frac{\partial v}{\partial x} + v\frac{\partial v}{\partial y} = -\frac{1}{\rho}\frac{\partial p}{\partial y}, \tag{2.3}$$

where u and v are the velocity components parallel and perpendicular to the main flow direction, and p and ρ denote the pressure and the density of the liquid. In the undisturbed case, the liquid flows in the x-direction with a uniform and steady velocity.

Indicating the upper and lower interfaces of the sheet by $y_+(x,t)$ and $y_-(x,t)$, we define the centreline position and the thickness of the sheet by

$$\overline{y}(x,t) = (y_+ + y_-)/2, \quad \tilde{y}(x,t) = y_+ - y_-\,. \tag{2.4}$$

The boundary conditions at the interfaces of the sheet are given by the following kinematic and dynamic conditions:
kinematic conditions

$$v_\pm = \frac{\partial y_\pm}{\partial t} + u_\pm \frac{\partial y_\pm}{\partial x}; \tag{2.5}$$

dynamic conditions

$$p_\pm = \pm\frac{\sigma}{R_\pm} = \mp\sigma f_\pm \frac{\partial^2 y_\pm}{\partial x^2} \quad \text{with} \quad f_\pm = \left[1 + \left(\frac{\partial y_\pm}{\partial x}\right)^2\right]^{-3/2}, \tag{2.6}$$

where the subscripts $+$ and $-$ denote values at the upper and lower interface, respectively. In (2.6), $R_\pm$ is the local radius of curvature of the interface and σ denotes the surface tension coefficient of the liquid. The ambient gas density and pressure are considered negligible, i.e. the limit of a void surrounding the liquid is considered. Vaporization is neglected.

Now, for a sheet whose thickness is small compared to the wavelength of a disturbance, it is convenient to reduce the problem to a one-dimensional unsteady

formulation. Equations (2.10), (2.11), (2.17), and (2.18) will be the leading-order equations resulting from a power-series expansion of the dependent variables u, v and p in terms of $(y - \overline{y})$. The same result can be obtained in a more *ad-hoc* fashion by (standard) one-dimensional approximations to the two-dimensional flow governed by (2.1)–(2.6) (Mehring & Sirignano 1998*a*). See also the analysis by Ramos (1992) for annular sheets in this context.

If u, v and p are analytical in x, y and t, then they are also analytical in x, $y - \overline{y}(x,t)$, and t provided that $\overline{y}$ is analytical. In this case we can employ the following expansions for the dependent variables:

$$u = u_0(x,t) + u_1(x,t)[y - \overline{y}(x,t)] + u_2(x,t)[y - \overline{y}(x,t)]^2 + \cdots, \tag{2.7}$$

$$v = v_0(x,t) + v_1(x,t)[y - \overline{y}(x,t)] + v_2(x,t)[y - \overline{y}(x,t)]^2 + \cdots, \tag{2.8}$$

$$p = p_0(x,t) + p_1(x,t)[y - \overline{y}(x,t)] + p_2(x,t)[y - \overline{y}(x,t)]^2 + \cdots, \tag{2.9}$$

where $|y - \overline{y}(x,t)| \leqslant |y_{\pm}(x,t) - \overline{y}(x,t)|$. The proposed polynominal expansion of u, v and p in terms of $[y - \overline{y}(x,t)]$ is a generalization of the series expansions in terms of the undisturbed sheet thickness h previously employed by other authors for the dilational case only (Matsuuchi 1976; Erneux & Davis 1993; Ramos 1996).

Inserting (2.7) and (2.8) into the expression for $(v_+ + v_-)/2$ given by (2.5) and considering $\tilde{y} = y_+ - y_-$ and $\overline{y} = (y_+ + y_-)/2$ yields

$$v_0 = \frac{\partial \overline{y}}{\partial t} + u_0 \frac{\partial \overline{y}}{\partial x} \tag{2.10}$$

for the transverse velocity component v to the lowest order in $(y - \overline{y})$. Equation (2.10) is accurate through first order in $|y_{\pm} - \overline{y}| = \tilde{y}/2$. Proceeding in the same way to express the velocity difference $(v_+ - v_-)$, one arrives at

$$\left(\frac{\partial \tilde{y}}{\partial t} + u_0 \frac{\partial \tilde{y}}{\partial x}\right) \frac{1}{\tilde{y}} = v_1 - u_1 \frac{\partial \overline{y}}{\partial x},$$

which is also accurate through order $|y_{\pm} - \overline{y}| = \tilde{y}/2$. The previous equation can be combined with the lowest-order equation in the series expansion of (2.1), i.e.

$$\frac{\partial u_0}{\partial x} - u_1 \frac{\partial \overline{y}}{\partial x} + v_1 = 0,$$

to yield

$$\frac{\partial \tilde{y}}{\partial t} + \frac{\partial (u_0 \tilde{y})}{\partial x} = 0. \tag{2.11}$$

The lowest-order approximation of (2.2) is obtained by replacing u, v and p by the appropriate series expansions and is given by

$$\frac{\partial u_0}{\partial t} + u_0 \frac{\partial u_0}{\partial x} = -\frac{1}{\rho}\left(\frac{\partial p_0}{\partial x} - p_1 \frac{\partial \overline{y}}{\partial x}\right). \tag{2.12}$$

A similar procedure to that described for the momentum equation in the axial direction (2.2) can be employed to obtain the lowest-order approximation to the momentum equation in the transverse direction (2.3). The final result here is

$$\frac{\partial v_0}{\partial t} + u_0 \frac{\partial v_0}{\partial x} = -\frac{p_1}{\rho}. \tag{2.13}$$

Equations (2.10), (2.11), (2.12) and (2.13) govern the relationships amongst u_0, v_0, $\tilde{y}$,

$\overline{y}$, p_0 and p_1. Equation (2.6) can now be used to obtain a closed system of equations governing the nonlinear wave distortion of thin liquid sheets.

Considering terms up to first order in the expansion of the pressure at the liquid interfaces $p_\pm$, i.e. $p_\pm = p_0 \pm p_1\,\tilde{y}/2$, one obtains $p_0 = (p_+ + p_-)/2$ and $p_1\,\tilde{y} = p_+ - p_-$ which can be expressed in terms of $\tilde{y}$ and $\overline{y}$ by employing (2.6), i.e.

$$p_0 = \frac{p_+ + p_-}{2} = -\frac{\sigma}{2}\left[\frac{f_+ + f_-}{2}\frac{\partial^2\tilde{y}}{\partial x^2} + (f_+ - f_-)\frac{\partial^2\overline{y}}{\partial x^2}\right], \tag{2.14}$$

$$p_1\,\tilde{y} = p_+ - p_- = -\sigma\left[(f_+ + f_-)\frac{\partial^2\overline{y}}{\partial x^2} + \frac{f_+ - f_-}{2}\frac{\partial^2\tilde{y}}{\partial x^2}\right], \tag{2.15}$$

where f_+ and f_- are given by

$$f_\pm = \left[1 + \left(\frac{\partial\overline{y}}{\partial x}\right)^2 \pm \frac{\partial\overline{y}}{\partial x}\frac{\partial\tilde{y}}{\partial x} + \frac{1}{4}\left(\frac{\partial\tilde{y}}{\partial x}\right)^2\right]^{-3/2}. \tag{2.16}$$

After insertion of (2.14), (2.15) and (2.16) into (2.12) and (2.13), the momentum equations in the axial and transverse directions take the following forms:

$$\frac{\partial u_0}{\partial t} + u_0\frac{\partial u_0}{\partial x} = \frac{\sigma}{2\rho}\left\{\frac{\partial}{\partial x}\left[\frac{f_+ + f_-}{2}\frac{\partial^2\tilde{y}}{\partial x^2} + (f_+ - f_-)\frac{\partial^2\overline{y}}{\partial x^2}\right] - \frac{2}{\tilde{y}}\frac{\partial\overline{y}}{\partial x}\left[(f_+ + f_-)\frac{\partial^2\overline{y}}{\partial x^2} + \frac{f_+ - f_-}{2}\frac{\partial^2\tilde{y}}{\partial x^2}\right]\right\}, \tag{2.17}$$

$$\frac{\partial v_0}{\partial t} + u_0\frac{\partial v_0}{\partial x} = \frac{\sigma}{\rho}\frac{1}{\tilde{y}}\left\{(f_+ + f_-)\frac{\partial^2\overline{y}}{\partial x^2} + \frac{f_+ - f_-}{2}\frac{\partial^2\tilde{y}}{\partial x^2}\right\}. \tag{2.18}$$

Equations (2.10), (2.11), (2.17), and (2.18) form a closed system of equations which together with appropriate boundary and initial conditions governs the nonlinear distortion of thin liquid sheets in a void.

The analysis of the nonlinear sheet distortion, governed by the above equations, is simplified by introducing non-dimensional quantities,

$$x^* = \frac{x}{l_{ref}},\ t^* = \frac{t}{l_{ref}/u_{ref}},\ y = \frac{\tilde{y}}{l_{ref}},\ Y = \frac{\overline{y}}{l_{ref}},\ u = \frac{u_0}{u_{ref}} \text{ and } \quad v = \frac{v_0}{u_{ref}}. \tag{2.19}$$

Also, derivation of the above governing equations in terms of non-dimensional variables and with disturbance wavelength λ as characteristic length l_{ref} shows that, (2.10), (2.11), (2.17) and (2.18) are exact in the limit where the ratio between undisturbed sheet thickness h and λ reaches zero, if $|y_\pm - \overline{y}| = O(h/2)$.

Using (2.19) to rewrite (2.10), (2.11), (2.17) and (2.18) yields the following non-dimensional system of equations:

$$\frac{\partial y}{\partial t^*} + \frac{\partial}{\partial x^*}(uy) = 0, \tag{2.20}$$

$$\frac{\partial u}{\partial t^*} + u\frac{\partial u}{\partial x^*} = \varepsilon^2\left\{\frac{\partial}{\partial x^*}\left[\frac{f_+ + f_-}{2}\frac{\partial^2 y}{\partial x^{*2}} + (f_+ - f_-)\frac{\partial^2 Y}{\partial x^{*2}}\right] - \frac{2}{y}\frac{\partial Y}{\partial x^*}\left[(f_+ + f_-)\frac{\partial^2 Y}{\partial x^{*2}} + \frac{f_+ - f_-}{2}\frac{\partial^2 y}{\partial x^{*2}}\right]\right\}, \tag{2.21}$$

$$\frac{\partial v}{\partial t^*} + u\frac{\partial v}{\partial x^*} = \varepsilon^2 \frac{2}{y}\left\{(f_+ + f_-)\frac{\partial^2 Y}{\partial x^{*2}} + \frac{f_+ - f_-}{2}\frac{\partial^2 y}{\partial x^{*2}}\right\}, \tag{2.22}$$

$$\frac{\partial Y}{\partial t^*} + u\frac{\partial Y}{\partial x^*} = v, \tag{2.23}$$

where $\varepsilon^2 = \sigma/(2\rho u_{ref}^2 l_{ref})$ and

$$f_\pm = \left[1 + \left(\frac{\partial Y}{\partial x^*}\right)^2 \pm \frac{\partial Y}{\partial x^*}\frac{\partial y}{\partial x^*} + \frac{1}{4}\left(\frac{\partial y}{\partial x^*}\right)^2\right]^{-3/2}. \tag{2.24}$$

Note that the symbols y, u and v defined in (2.19) now have a different meaning from those employed in (2.1), (2.2) and (2.3).

Expressing the flow variables y, Y, u and v within the above equations in terms of their undisturbed and fluctuating values, the corresponding linearized system of equations is readily obtained by neglecting terms which contain products of the fluctuating quantities. The linearized system of equations is given by

$$\frac{\partial y'}{\partial t^*} + u^{(0)}\frac{\partial y'}{\partial x^*} + y^{(0)}\frac{\partial u'}{\partial x^*} = 0, \tag{2.25}$$

$$\frac{\partial u'}{\partial t^*} + u^{(0)}\frac{\partial u'}{\partial x^*} = \varepsilon^2\frac{\partial^3 y'}{\partial x^{*3}}, \tag{2.26}$$

$$\frac{\partial v'}{\partial t^*} + u^{(0)}\frac{\partial v'}{\partial x^*} = \varepsilon^2\frac{4}{y^{(0)}}\frac{\partial^2 Y'}{\partial x^{*2}}, \tag{2.27}$$

$$\frac{\partial Y'}{\partial t^*} + u^{(0)}\frac{\partial Y'}{\partial x^*} = v', \tag{2.28}$$

where $y^{(0)}$ and $u^{(0)}$ or y' and u' denote the non-dimensional undisturbed or fluctuating values of the sheet thickness y and the sheet velocity u, respectively ($y = y^{(0)} + y'$, $u = u^{(0)} + u'$). The non-dimensional undisturbed transverse velocity component of the sheet $v^{(0)}$ and its non-dimensional undisturbed centreline location $Y^{(0)}$ are zero. The values of $y^{(0)}$ and $u^{(0)}$ are constant and will depend on the characteristic length and velocity scales chosen for the particular problem according to table 1. From (2.25)–(2.28), we see that, in the linear case, the dilational (or symmetric) mode of sheet distortion governed by (2.25) and (2.26) is decoupled from the sinuous (or antisymmetric) mode, the latter being governed by (2.27) and (2.28). This is in contrast to the nonlinear case governed by (2.20)–(2.23) where a coupling occurs.

The present analysis does not model the details of the sheet-disintegration process during the sheet breakup. Such an analysis would require a modification of the governing equations presented above, in order to include molecular forces that become important when the sheet thickness is of the order of the molecular mean free path. For symmetric periodically disturbed infinite sheets, such an analysis has been presented by Erneux & Davis (1993) and more recently by Vaynblat *et al.* (1997).

3. Infinite sheets

3.1. *Linear analysis*

Introducing the Galilean transformation defined by

$$\tau = t^*, \quad \xi = x^* - u^{(0)}t^* \tag{3.1}$$

and choosing l_{ref} to be the undisturbed sheet thickness h, and $u_{ref} = (\sigma/(2\rho h))^{1/2}$ (so that $\varepsilon = 1$), equations (2.25) and (2.26) or (2.27) and (2.28) can be combined to yield

$$\frac{\partial^2 y'}{\partial \tau^2} + \frac{\partial^4 y'}{\partial \xi^4} = 0, \tag{3.2}$$

$$\frac{\partial^2 Y'}{\partial \tau^2} - 4\frac{\partial^2 Y'}{\partial \xi^2} = 0. \tag{3.3}$$

Equations (3.2) and (3.3) illustrate that the dilational and sinuous distortions of thin liquid sheets in a void are decoupled and do not interact in a linear analysis. However, the undisturbed sheet thickness, that has been chosen as the characteristic length in the non-dimensionalization process, is a scaling factor for both dilational and sinuous cases. Equations (3.2) and (3.3) are both well-known equations in dynamical mechanics, governing the transverse vibration of a uniform beam and vibrations on a taut string, respectively. The propagation characteristics of free waves and waves resulting from forced motion on both beams and strings have been analysed extensively in the literature (Graff 1975; Ortner 1978). Within the analysis of thin liquid sheets, Taylor (1959*a*) first derived and analysed (3.2) and (3.3), the latter in its steady form and for a radially expanding planar sheet.

Periodic travelling wave solutions to (3.2) for the dilational case are readily obtained by separation of variables. The reciprocal relation between the disturbance wavelength λ_d^* and the wave velocity V_d^* (i.e. $V_d^* = 2\pi/\lambda_d^*$) observed in this linear case illustrates the dispersive nature of the dilational sheet distortion. It indicates that the dimensional wave velocity is proportional to the factor $(\sigma h/2\rho)^{1/2}$ divided by the wavelength λ. This implies that the short wavelengths travel faster. In fact, the phase velocity increases without limit for decreasing wavelength. This anomaly is a result of the inviscid flow assumption and has already been observed for the (linear) transverse vibration of beams where it is a consequence of neglecting rotary inertia and shear effects (Graff 1975). It should be noted however that the theory employed here is only valid for thin sheets, i.e. where the wavelength of the imposed sheet disturbance is large compared to the sheet thickness. Travelling wave solutions to (3.3) show that (linear) sinuous capillary waves on thin sheets are non-dispersive, with a constant wave velocity of $V_s^* = 2$. Comparison of the linear wave velocities V^* for sinuous and dilational waves also shows that on thin sheets, i.e. $\lambda^* \gg 1$, sinuous (or antisymmetric) waves propagate much faster than dilational waves. The results described here, obtained by using a reduced-dimension approach, were presented by Taylor (1959*a*), and can also be obtained by taking the linearized two-dimensional solution of Squire (1953) or Rangel & Sirignano (1991) in the limit of a thin layer with zero ambient gas density. Apart from the single-harmonic wave analyses described above, more general analyses of the free and forced motion of infinite and finite media governed by (3.2) and (3.3) were described by Graff (1975).

3.2. *Nonlinear exact analysis* (*dilational thin sheet case*)

The analysis in this section is a modification of the analysis by Sirignano & Mehring (1996). For dilational sheet disturbances only, we have $\overline{y} = (y_+ + y_-)/2 = 0$ or $v_0 = \partial\overline{y}/\partial t + u_0\,\partial\overline{y}/\partial x = 0$, so that after employing non-dimensionalization and a Galilean transformation, the nonlinear system of equations (2.20)–(2.23) reduces to

$$\frac{\partial y}{\partial \tau} + \frac{\partial (yu')}{\partial \xi} = 0, \tag{3.4}$$

$$\frac{\partial u'}{\partial \tau} + u' \frac{\partial u'}{\partial \xi} = \frac{\partial}{\partial \xi}\left[q \frac{\partial^2 y}{\partial \xi^2}\right], \tag{3.5}$$

with $q = f_+ = f_- = [1 + \frac{1}{4}(\partial y/\partial \xi)^2]^{-3/2}$. The assumption of travelling wave solutions, i.e.

$$y = F(\zeta) = F(\xi - V^*\tau), \quad u' = G(\zeta) = G(\xi - V^*\tau) \tag{3.6}$$

then yields, after insertion into (3.4) and (3.5),

$$\left(G - V^*\right) \frac{\mathrm{d}F}{\mathrm{d}\zeta} + F \frac{\mathrm{d}G}{\mathrm{d}\zeta} = 0, \tag{3.7}$$

$$\left(G - V^*\right) \frac{\mathrm{d}G}{\mathrm{d}\zeta} - \frac{\mathrm{d}}{\mathrm{d}\zeta}\left[q \frac{\mathrm{d}^2 F}{\mathrm{d}\zeta^2}\right] = 0. \tag{3.8}$$

Integration of (3.7) provides $G = u' = V^*\left(1 - 1/F\right)$ where the integration constant is obtained by adjusting the Galilean transformation so that $G = 0$ when $F = 1$. This implies that the product of the liquid velocity (relative to the moving wave) and the thickness remains constant. Introducing this result into (3.8) gives

$$\frac{V^{*2}}{F^3} \frac{\mathrm{d}F}{\mathrm{d}\zeta} + \frac{\mathrm{d}}{\mathrm{d}\zeta}\left[q \frac{\mathrm{d}^2 F}{\mathrm{d}\zeta^2}\right] = 0. \tag{3.9}$$

Integration of (3.9) yields

$$K - \frac{V^{*2}}{2F^2} + q \frac{\mathrm{d}^2 F}{\mathrm{d}\zeta^2} = 0, \tag{3.10}$$

where K is the constant of integration. We will choose the reference length here so that $F = 1$ at the point where the second derivative is zero. This will determine $K = V^{*2}/2$. The reference length now is not the unperturbed thickness but goes to that value as the amplitude of the wave goes to zero. Later, we shall determine this reference-length value. Now we multiply (3.10) by $\mathrm{d}F = (\mathrm{d}F/\mathrm{d}\zeta)\mathrm{d}\zeta$ and integrate with respect to ζ. This yields

$$\left[1 + \frac{1}{4}\left(\frac{\mathrm{d}F}{\mathrm{d}\zeta}\right)^2\right]^{-1/2} = V^{*2} H(F, c), \tag{3.11}$$

where $H(F, c)$ has been defined as $H(F, c) = \frac{1}{8}[(F + 1/F) + c]$ and c is a constant of integration. For a soliton-type solution, $\mathrm{d}F/\mathrm{d}\zeta \to 0$ and $F \to 1$ as $\zeta \to -\infty$; whereas for a periodic solution, $\mathrm{d}F/\mathrm{d}\zeta = 0$ at maximum and minimum values of F. Therefore, $c = 1/V^{*2} - \frac{1}{4}$ for a soliton-type solution and

$$H(F_{max}, c) = H(F_{min}, c) = 1/V^{*2} \tag{3.12}$$

for periodic solutions.

It follows that $F_{min} = F_{max} = 1$ for a soliton solution; this implies $F = 1$ everywhere so that no soliton wave can exist. Therefore, we consider only periodic disturbances. Note that solutions with discontinuous first or second derivatives are not considered; otherwise discontinuities in the surface-tension force and pressure could occur.

Equation (3.11) indicates that, for any value of F, two values of its slope exist with equal magnitude but opposite sign. This implies that symmetries exist for $F(\zeta)$ about the maximum and minimum points. Note that (3.12) gives $c = 1/V^{*2} - \frac{1}{4}$ for the trivial case where $F_{max} = F_{min} = 1$.

To find the solution $y = F(\zeta) = F(\xi - V^*\tau)$, (3.11) is rewritten in the form

$$\frac{\mathrm{d}F}{\mathrm{d}\zeta} = \pm 2\left[\frac{1}{V^{*4}H(F,c)^2} - 1\right]^{1/2} \quad \text{or} \quad \mathrm{d}\zeta = \pm\frac{1}{2}\left[\frac{1}{V^{*4}H(F,c)^2} - 1\right]^{-1/2}\mathrm{d}F$$

and integrated starting at $\zeta = 0$ with $F_m = F_{min}$ or F_{max}. The resulting integral equation

$$\int_0^{\zeta}\mathrm{d}\zeta' = \frac{1}{2}\int_{F_m}^{F}\left[\frac{1}{V^{*4}H(F',c)^2} - 1\right]^{-1/2}\mathrm{d}F' \tag{3.13}$$

then provides the exact solution $y = F(\zeta)$ to (3.9). In (3.13) a minus sign appears in front of the integrand wherever $\mathrm{d}F/\mathrm{d}\zeta$ is negative.

From (3.13), the wavelength in ζ-space λ_ζ can be determined as

$$\lambda_\zeta = \int_{F_{min}}^{F_{max}}\left[\frac{1}{V^{*4}H(F,c)^2} - 1\right]^{-1/2}\mathrm{d}F. \tag{3.14}$$

In order to determine the reference length, we can employ the conservation-of-mass principle. The normalized unperturbed thickness a is given by

$$a\,\lambda_\zeta = \int_0^{\lambda_\zeta} F\mathrm{d}\zeta. \tag{3.15}$$

From (3.14) and (3.15), a is governed by the relationship

$$\int_{F_{min}}^{F_{max}}\left[\frac{1}{V^{*4}H(F,c)^2} - 1\right]^{-1/2}(F-a)\,\mathrm{d}F = 0\,. \tag{3.16}$$

Since a is the ratio of the dimensional unperturbed thickness to the reference length, the reference length is known once (3.16) is solved. The thickness normalized by the unperturbed thickness is given by F/a. It can be shown that the velocity for the Galilean transformation is the product of a and the unperturbed velocity.

We can arrive at an approximate solution to (3.9) by first expanding the quantity within brackets in (3.11)

$$1 - \frac{1}{8}\left(\frac{\mathrm{d}F}{\mathrm{d}\zeta}\right)^2 + \frac{3}{128}\left(\frac{\mathrm{d}F}{\mathrm{d}\zeta}\right)^4 - \cdots = V^{*2}H(F,c). \tag{3.17}$$

If we take only the two leading terms in the above expansion, it is equivalent to approximating $q \approx 1$ in (3.5) and (3.9). In that case, we can make the analogy with a simple oscillator and relate the left-hand side of (3.17) to a kinetic energy term and the right-hand side to a total energy less the potential energy. However, in physical terms, the analogy is very poor since just the opposite is true; the left-hand side derives from the surface-tension forces while the right-hand side derives from the inertial term. Furthermore, (3.11) is a statement of momentum balance rather than a statement of energy balance.

Using the approximation $q \approx 1$ and employing the same procedure as for the derivation of the exact solution (3.13), (3.17) yields after separation and integration

$$\int_0^{\zeta}\mathrm{d}\zeta' = \frac{1}{|V^*|}\int_{F_m}^{F}\frac{\mathrm{d}F'}{(C - (1/F' + F'))^{1/2}}, \tag{3.18}$$

where again a minus sign appears in front of the integrand wherever the slope $\mathrm{d}F/\mathrm{d}\zeta$ is negative. Note that, for both the exact solution and the above approximate

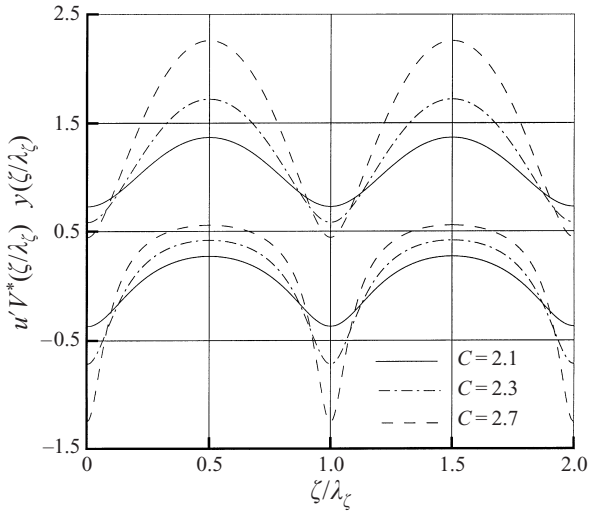

FIGURE 1. Nonlinear travelling wave solution $y = F(\zeta/\lambda_\zeta, C)$ governed by (3.18). λ_ζ denotes the non-dimensional wavelength of the solution and $u'/V^* = 1 - 1/F$ the corresponding streamwise velocity.

solution, F_{min} and F_{max} are functions of the integration constant C (e.g. $F_{min,max} = (C \mp (C^2 - 4)^{1/2})/2$) or equivalently of c. This demonstrates the significance of either of these constants as an amplitude parameter in the solutions (3.13) and (3.18).

From (3.18) the wavelength λ_ζ is given by

$$\lambda_\zeta = \frac{2}{|V^*|} \int_{F_{min}}^{F_{max}} \frac{\mathrm{d}F}{(C - (1/F + F))^{1/2}}, \tag{3.19}$$

which is correct through second order in the amplitude of the derivative $\mathrm{d}F/\mathrm{d}\zeta$; the error is third order. From the approximate solution for λ_ζ we note that, once C and the wave velocity V^* are specified, the amplitude and wavelength of the nonlinear travelling wave are determined. This is in contrast to the linear case, where dilational travelling waves have the same propagation velocity at any disturbance amplitude. However, (3.19) also reveals that the linear result $V_d^* \sim 1/\lambda_d^*$ also applies in the nonlinear case and is correct through second order in the amplitude of the derivative $\mathrm{d}F/\mathrm{d}\zeta$. The product of wavelength and wave speed is weakly dependent on the wave amplitude and, in linear theory, becomes independent of the amplitude for the dispersive dilational travelling wave.

Figure 1 illustrates the nonlinear travelling wave solutions given by (3.18) for different values of C.

After performing the above analysis of nonlinear dilational travelling waves, a careful literature review revealed the existence of a similar analysis attempted by Matsuuchi (1974, 1976). Matsuuchi chose the two integration constants appearing in the integration process of the nonlinear governing equations freely and independently which allows for nonlinear dilational travelling waves with independent values for the maximum and minimum sheet thickness. However, as shown above, consideration of the trivial solution, i.e. $(u' = 0, y = 1)$, can be used to determine one of the integration constants. This leaves only one free constant, i.e. c or C, which determines both the minimum and maximum amplitude of the travelling nonlinear wave, rendering them dependent on each other.

In conclusion of this analysis, we find that nonlinear capillary wave trains of constant amplitude can exist on thin liquid sheets if a relation such as (3.19) is satisfied among the wave amplitude (represented by C), the wavelength and the wave velocity (see also figure 1). Furthermore, (3.19) also reveals that for dilational waves, the nonlinearity leads to a decrease in the wave velocity which is contrary to the case of gravity waves (Lamb 1932). The same findings were also reported by Matsuuchi (1976).

3.3. *Nonlinear numerical analysis*

Equations (2.20)–(2.23) have been solved numerically as an initial-value problem and with periodicity conditions imposed at the boundaries of the computational domain. Non-dimensional numerical simulations were performed in the same reference frame as the linear solutions presented earlier. For the non-dimensionalization the same reference length and velocity were used as in the linear case. Numerical solutions were obtained by using the Lax–Wendroff method with Richtmyer splitting (Ferziger 1981). This followed a suggestion by I. Kim (1997, personal communication). See also Kim & Sirignano (1997). In the linear limit, the latter reduces to the ordinary Lax–Wendroff method.

3.3.1. *Dilational case*

To validate the implementation of the numerical scheme, the propagation of the nonlinear waves governed by (3.18) was considered. To be consistent in the comparison of this approximate analytical solution with the corresponding numerical results, the approximation $q \approx 1$ was also employed in the numerical solution of the appropriate non-dimensional equations (but only for this validation exercise), i.e. (3.4) and (3.5).

Figure 2 illustrates the numerical result obtained for such a wave ($C = 2.5$ and $V^* = 1 \rightarrow \lambda^* \approx 6.865$). The appropriate initial conditions for this case are $y(\tau = 0, \xi) = F(\xi, C = 2.5)$ and $u'(\tau = 0, \xi) = V^*(1 - 1/F)$, where F is given by (3.18) with $\zeta = \xi$ at $\tau = 0$ according to (3.6). The number of grid points per disturbance wavelength was $n_\xi = 100$ and the integration time step per time period $T = \lambda^*/V^*$, $\Delta\tau/T = 10^{-4}$.

One observes that the shape of the periodic nonlinear travelling wave is very well preserved in the numerical simulation, and the velocity at which the wave travels agrees with the analytical prediction. This result has been confirmed for a wide range of (nonlinear) waves, i.e. waves with different amplitudes (or C-values) and propagation velocities V^* (not illustrated). For very small wave amplitudes (i.e. $C \rightarrow 2$), analytical and finite-difference solutions were also found to agree with the results obtained from the linear analysis. The nonlinear waves governed by (3.18) are stable with regard to disturbances introduced by the numerical scheme employed.

The influence of nonlinear effects on symmetric distorting sheets was analysed by comparison of linear analytical and nonlinear numerical solutions for various initial conditions of harmonically disturbed (infinite) sheets. Initial conditions were chosen to be travelling wave solutions of the linear equation (3.2), i.e.

$$y_d(\tau, \xi) = 1 + A_d \cos\left[\frac{2\pi}{\lambda^*}(\xi - V^*\tau)\right] \quad \text{at} \quad \tau = 0, \tag{3.20}$$

where A_d denotes the (non-dimensional) disturbance amplitude, and where the wave velocity V^* and the time period T are given by $V^* = 2\pi/\lambda^*$ and $T = \lambda^*/V^* = \lambda^{*2}/(2\pi)$ as described earlier. The initial momentum disturbance of the sheet for the specified sheet disturbance is obtained from the above expression for $y_d(\tau = 0, \xi)$ and the

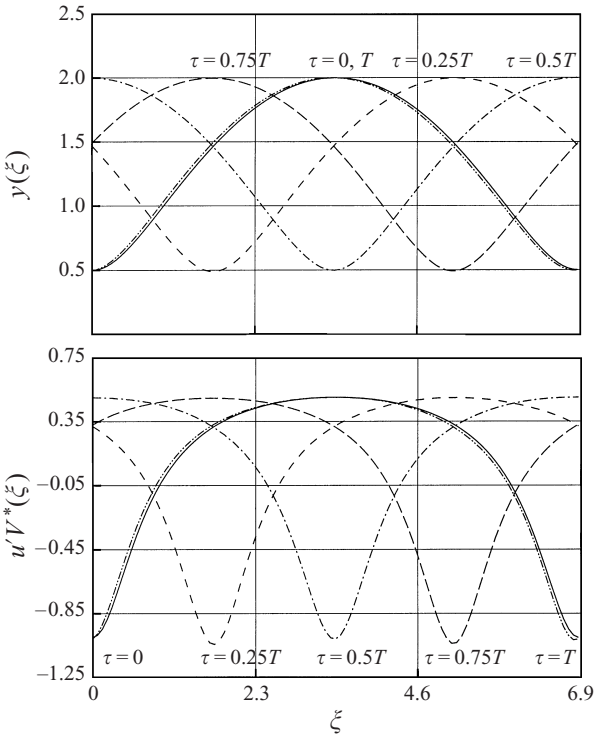

FIGURE 2. Numerical solution for a propagating nonlinear dilational travelling wave governed by (3.18) ($V^* = 1$, $C = 2.5 \rightarrow \lambda^* \approx 6.865$).

linearized continuity equation (2.25) after Galilean transformation, i.e.

$$u'_d = V^* A_d \cos\left[\frac{2\pi}{\lambda^*}\xi\right]. \tag{3.21}$$

For all the simulations, the number of grid points per wavelength λ^* was $n_\xi = 200$ and the integration time step per time period T, $\Delta\tau/T = 10^{-4}$. Figure 3 illustrates the linear and nonlinear wave propagation for the case $A_d = 0.55$.

Comparison between linear and nonlinear results shows that nonlinear effects induce a slight temporal oscillation of the disturbance amplitude, combined with an increased thinning of the sheet and a pulsating steepening and de-steepening on the front or back of the wave ('wobbling'). For the nonlinear dilational wave propagation on an infinite sheet, the difference between the exact solution with its constant waveform and the wave resulting from the initial sinusoidal thickness variation can be described by the higher harmonics. Since the wave phenomenon is dispersive, these higher harmonics do not travel at the same speed as the fundamental component. Therefore, an unsteady waveform results. The frequency at which the sheet alternately steepens at one side and flattens at the opposite side is of the same order as the oscillation frequency of the maximum amplitude variation, since both originate in the presence of the higher harmonics. Figure 3 also reveals that the system nonlinearity effectively decreases the propagation velocity of the initially linear travelling wave. For the case illustrated in figure 3, the linear wave travels five wavelengths, while the nonlinear wave only propagates about 4 wavelengths (not illustrated).

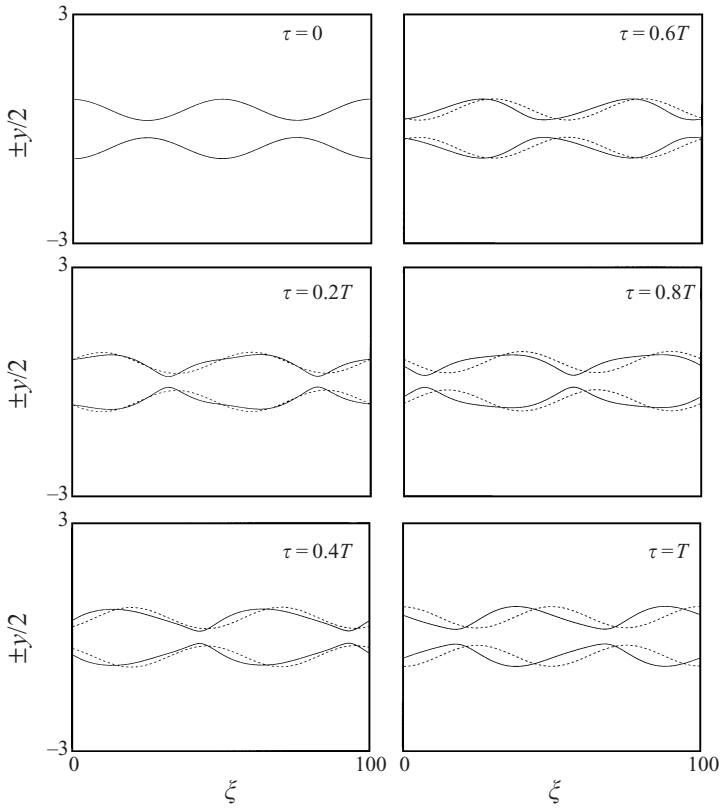

FIGURE 3. Linear and nonlinear propagation of a dilational travelling wave initially prescribed by (3.20) and (3.21) ($\lambda^* = 50, A_d = 0.55$: – – –, linear; ——, nonlinear; $0 < \tau < T$).

Figure 4 illustrates the evolution of an initially highly disturbed sheet ($A_d = 0.65$). In this case, as was found for all cases of $A_d > 0.61$ and $\lambda^* = 50$, the wave thins and breaks at a finite time due to nonlinear effects, i.e. due to the appearance of the previously described higher-harmonic waves which, in interaction with each other and the original wave disturbance, cause variations of the sheet thickness resulting in sheet disintegration since the original sheet disturbance is already very high. However, in all cases under consideration the nonlinearity did not promote sheet breakup due to severe wave steepening or amplitude growth of the travelling wave. We note that Rangel & Sirignano (1991) found amplitude growth for both linear and nonlinear analyses when the ambient gas density was not negligible; they also found severe wave steepening in the nonlinear case.

Nonlinear numerical simulations for various values of the non-dimensional disturbance wavelength $\lambda^* = \lambda/h$ showed that the time T_c typically required for one oscillation of the sheet in the transverse or axial direction increases monotonically as the non-dimensional wavelength λ^* is increased. However, the increase of T_c with increasing λ^* is less than the corresponding increase of the time period T of the travelling wave, since the nonlinear oscillation is associated with higher-harmonic dilational waves for which variations in T due to changes in λ^* are smaller than for the initially imposed disturbance with larger value of λ^*. (Note that, by linear analysis, $\mathrm{d}T/\mathrm{d}\lambda^* \sim \lambda^*$ for dilational waves.) The effect of variations of λ^* on the propagation velocity or time period T of the travelling wave describes the dispersive nature of

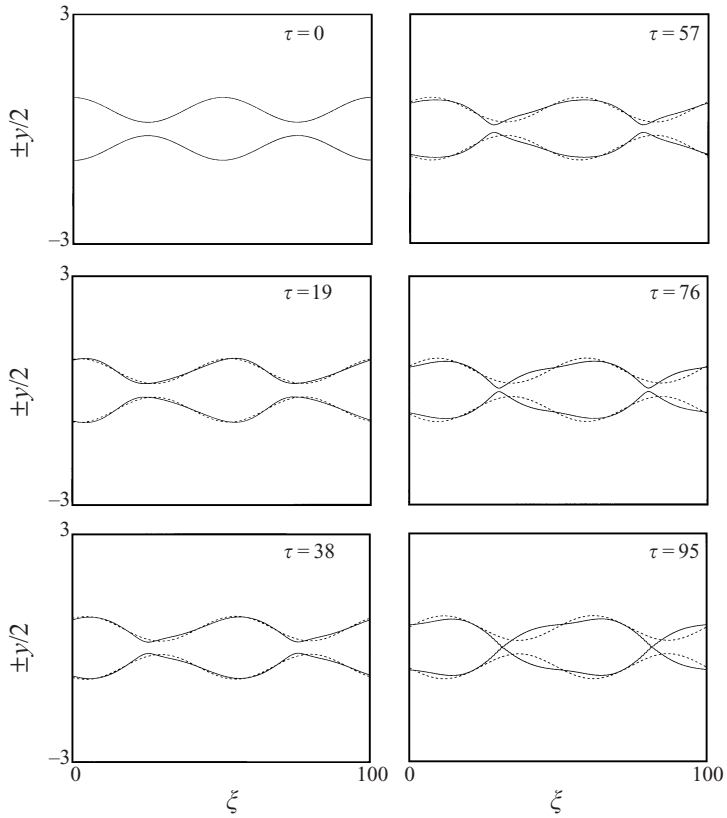

FIGURE 4. Linear and nonlinear propagation of a dilational travelling wave initially prescribed by (3.20) and (3.21) ($\lambda^* = 50, A_d = 0.65$: – – –, linear; ——, nonlinear).

the problem and was already discussed within the linear analysis. The importance of nonlinear effects on the deviation of the functional dependency of V^* from the linear case ($V^* = 2\pi/\lambda^*$) has not been analysed, except for the analytical nonlinear considerations presented earlier. No significant changes in the characteristics of the nonlinear sheet oscillation or its frequency were found with variations of the initial disturbance amplitude A_d (e.g. for $A_d = 0.61$) or at later times in the simulation (e.g. within $0 < \tau < 6T$).

Also, the analysis of standing waves created by the superposition of two initially linear travelling waves with opposite wave velocities but the same wavelengths and disturbance amplitudes showed that the existence of higher-harmonic waves in the nonlinear simulations leads at times to the formation of fluid lumps very similar to those observed on semi-infinite modulated sheets (see figure 13). This similarity might be explained by the fact that, as for the standing wave analysis, there are two waves present on the modulated semi-infinite sheet. In the case of figure 13, the two waves have slightly different wave speeds and wavenumbers.

Nonlinear effects such as those described above are only significant if the disturbance amplitude A_d is large enough. For the travelling-wave case with $\lambda^* = 50$, the limit where linear theory can be applied was found to be at $A_d \approx 0.4$.

The previous analysis showed that nonlinear effects do not support wave breaking or severe amplitude growth of initially linear dilational travelling waves. However,

severe amplitude growth can occur for the case where subharmonic dilational disturbances are superimposed on an already symmetrically disturbed sheet.

The existence of this 'modulational' instability, arising from the nonlinear interaction between different dilational modes, had already been observed and analysed by Matsuuchi (1974, 1976) and has also been observed in the present analysis for a variety of different initial conditions (i.e. initially linear and nonlinear travelling wave solutions with subharmonic disturbances at different amplitudes and wavelengths). However, the existence of the prescribed instability in the fully two-dimensional nonlinear case remains to be addressed. In this context, the use of the subsequently employed two-dimensional discrete-vortex method is problematic due to the increase of numerical error along the time-integration process, especially when using short time steps. These short time steps are required to allow for a sufficient number of point vortices in order to obtain an accurate spatial resolution of the problem. The significance of growing numerical error in discrete-vortex methods has been discussed elsewhere (Pullin 1982).

3.3.2. *Sinuous case*

To investigate the importance of nonlinear effects for sinuous distorting thin liquid sheets, the same approach is taken as for the investigation of dilational disturbances in the previous section, i.e. the same non-dimensionalization and Galilean transformation are employed. The corresponding non-dimensional equations to be solved are now given by (2.20)–(2.23) written in the appropriate coordinate system (ξ, τ) and with ε^2 and u replaced by 1 and u', respectively.

Linear analytical and nonlinear numerical solutions to these equations are compared for various initial conditions of sinuous (i.e. antisymmetric) periodically disturbed sheets. Analogous to the dilational case, initial conditions were chosen to be travelling wave solutions to the linearized equation (3.3), i.e.

$$Y_s = A_s \cos\left[\frac{2\pi}{\lambda^*}(\xi - V^*\tau)\right], \quad v_s = \frac{\partial Y_s}{\partial \tau} = A_s \frac{2\pi V^*}{\lambda^*} \sin\left[\frac{2\pi}{\lambda^*}(\xi - V^*\tau)\right] \quad \text{at} \quad \tau = 0, \tag{3.22}$$

with wave velocity $V^* = 2$ and time period $T = \lambda^*/V^*$ as described earlier. Initial conditions for u' and y are taken at their undisturbed values, i.e. $u'(\xi, \tau = 0) = 0$ and $y(\xi, \tau = 0) = 1$. Similarly to the dilational case, A_s denotes the (non-dimensional) amplitude of the sinuous sheet disturbance. For the numerical solution the same number of grid points per wavelength and time steps per time period were employed as for the corresponding dilational cases analysed earlier. Accuracy of the numerical solutions was assessed for both dilational and sinuous cases by successive refinement of mesh size and time step. The mesh size resulting from $n_\xi = 200$ grid points per disturbance wavelength λ^* and the time step $\Delta\tau = 10^{-4}\,T$ employed are rather small for the dilational case analysed earlier; however, they are required in order to provide appropriate spatial and temporal resolution for both sinuous and dilational cases under consideration.

Figure 5 illustrates the temporal evolution of a travelling wave initially prescribed by equation (3.22) with $A_s = 1.375$ and for $\lambda^* = 50$. Note that for $A_s = 0.55$ and $\lambda^* = 50$ as used previously for the illustrated dilational case, nonlinear effects are negligible (not illustrated). However, from figure 5 we see that nonlinear effects cause a considerable distortion and might even lead to the breakup of an initially linear sinuous travelling wave, if the disturbance amplitude A_s is large enough (figure 7). Comparison between linear and nonlinear solutions for the case shown in figure 5

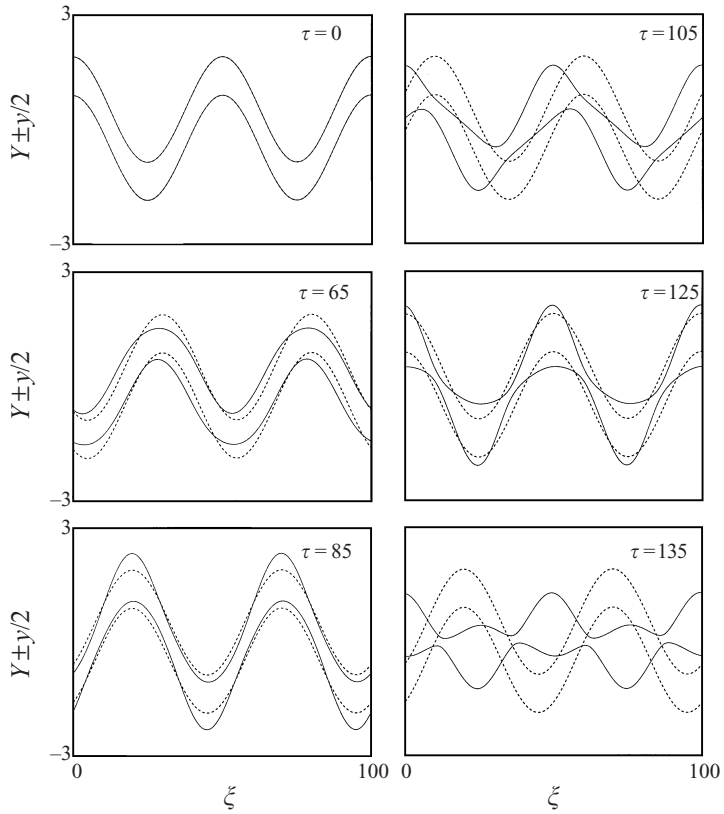

FIGURE 5. Linear and nonlinear propagation of a sinuous travelling wave initially prescribed by (3.22) ($\lambda^* = 50$, $A_s = 1.375$: – – –, linear; ——, nonlinear).

indicates that nonlinear effects become significant only after the sinuous wave has travelled about two wavelengths, i.e. for $\tau > 2T$. After this time the nonlinear effects were found to cause an oscillation of the sheet in the transverse flow direction at a frequency significantly greater than $1/T$.

Figure 5 at $\tau = 85$ shows that, in the nonlinear case, the transverse oscillation of the sheet is accompanied by an increase in the maximum disturbance amplitude of the wave together with an accumulation of fluid in the maximum deflection region of the sheet, which then results in a sawtooth-like sheet configuration rather than a sinuousoidal one. In particular, the nonlinear coupling between the sinuous and dilational modes causes variations in the sheet thickness with wavelengths about one-half of that for the initially imposed antisymmetric disturbance. The sheet distortion is dominated by the nonlinear interaction between the basic sinuous mode and a dilational first harmonic as described by Clark & Dombrowski (1972) with only minor contributions of higher-harmonic sinuous waves like those observed within the analysis by Jazayeri & Li (1996). Figure 5 illustrates that sheet thinning can occur at the location of maximum slope as found at times $\tau = 85$ and 125 or it might occur at points located near the maximum deflection region as at time $\tau = 105$. Only the latter has been described by other authors using nonlinear two-dimensional simulations (Rangel & Sirignano 1991), or higher-order expansions of the two-dimensional problem (Clark & Dombrowski 1972; Jazayeri & Li 1996).

The previously mentioned sheet oscillation in the transverse flow direction is clearly observed from the time sequence shown in figure 5. A similar observation was made by Rangel & Sirignano (1991) for the case of aerodynamically unstable planar sheets. (See Rangel & Sirignano 1991, figure 9.) The present results illustrate the existence of this nonlinear oscillation even in the absence of aerodynamic forces.

Standing-wave simulations analogous to those conducted for the dilational case discussed earlier (i.e. two travelling waves with opposite wave speeds but the same disturbance amplitudes and wavelengths) showed that, at the time where the maximum disturbance amplitude is reached, fluid agglomeration in the sheet edges is increased in comparison to the case with only one travelling wave. The same observation can be made in the case of sinuous modulated sheets where the imposed modulation results in the appearance of one or two downstream travelling waves. See figures 16 and 17.

Nonlinear effects such as those described above increase as the disturbance amplitude of the travelling wave solution imposed at $\tau = 0$ is increased. For very small values of the amplitude A_s, the linear solution is recovered, i.e. the initially imposed linear travelling wave solution preserves its shape throughout the simulation and travels with the velocity $V^* = 2$ predicted by linear theory. However, for initially sinuous travelling waves with very high disturbance amplitudes, nonlinear effects might cause the sheet to break up at points interspaced by half a wavelength and located near the maximum deflection region of the sheet. (See figure 7.) This is analogous to the numerical results presented by Rangel & Sirignano (1991) for a very low density-ratio value of 0.01 (Rangel & Sirignano 1991, figure 6). It also agrees with the experimental observations made by Mansour & Chigier (1990, figure 15) and suggests that, for the case of a liquid sheet in a co-flowing gas stream, as considered by the previously mentioned authors, the nonlinear coupling between dilational and sinuous modes causes the sheet to break up, after aerodynamic interaction caused the oscillation amplitude of the sinuous distorting sheet to increase sufficiently for the prescribed nonlinear interaction to 'take over'. Both the linear and the nonlinear solutions maintain their antisymmetric character with time, i.e. $Y(\xi, \tau) = -Y(\xi + \lambda^*/2, \tau)$ and $y(\xi, \tau) = y(\xi + \lambda/2, \tau)$.

3.3.3. *Comparison with nonlinear two-dimensional simulations*

In order to benchmark the accuracy of the proposed reduced-dimension approach, nonlinear one-dimensional results have been compared to fully two-dimensional nonlinear computations using the discrete-vortex method described by Rangel & Sirignano (1991). Initial conditions for both nonlinear two-dimensional and one-dimensional simulations were obtained from the solution to the linear two-dimensional problem already presented by these authors. The latter shows that the linear motion of a two-dimensional liquid sheet in a void is always stable. Also, for the case of a liquid sheet in a gas of zero density, the two-dimensional linear analysis presented by Rangel & Sirignano (1991) reduces to the linear analysis described earlier in the limit where the ratio between the undisturbed sheet thickness and the disturbance wavelength approaches zero.

For easy comparison between the different numerical results, the length and time scales for non-dimensionalization in both the one-dimensional and two-dimensional approaches are chosen to be the same. This requires some adjustment of the non-dimensionalization schemes described before and employed by Rangel & Sirignano (1991); it also implies that the Weber number for both one-dimensional and two-dimensional simulations will be $We = 1$. Both simulations are performed in a frame of reference which is moving with the undisturbed sheet velocity. The spatial and

	2D-vortex code	1D-approach
u_{ref}	U	$(\sigma/(2\rho l_{ref}))^{1/2}$
l_{ref}	λ	h
t_{ref}	l_{ref}/u_{ref}	l_{ref}/u_{ref}

TABLE 1. Characteristic velocities, lengths and time scales ($u_{ref}, l_{ref}, t_{ref}$) used within the discrete-vortex method by Rangel & Sirignano (1991) and employed previously within the reduced-dimension approach.

temporal coordinates employed are therefore ξ and τ according to (3.1). This is in contrast to the work by Rangel & Sirignano (1991) where the authors have chosen a reference frame in which the undisturbed fluid sheet moves with velocity $-U/2$ and the surrounding semi-infinite gas streams move with velocity $U/2$. Note that since there is no interaction between the fluid sheet considered and its surrounding void, the undisturbed sheet velocity or the relative velocity U between the sheet and its surrounding is not a parameter in this analysis. Table 1 shows the characteristic lengths and velocities used in the non-dimensionalization process of the previous reduced-dimension analyses, as well as in the non-dimensional discrete-vortex method by Rangel & Sirignano (1991). Note that the choice of $u_{ref} = (\sigma/(2\rho l_{ref}))^{1/2}$ eliminated the Weber number as part of the non-dimensional equations in the one-dimensional case. The same can be done in the two-dimensional case, if the Weber number $We = \rho u_{ref}^2 l_{ref}/\sigma$ is defined by using $u_{ref} = (\sigma/\rho\lambda)^{1/2}$ rather than $u_{ref} = U$ as employed by Rangel & Sirignano (1991).† Therefore, assuming $l_{ref,1D} = \lambda$ and $u_{ref,1D} = (\sigma/(\rho\lambda))^{1/2}$ within the one-dimensional analysis provides the same length and velocity scales for both one-dimensional and two-dimensional simulations, if $u_{ref,2D}$ is chosen accordingly ($u_{ref,2D} = (\sigma/\rho\lambda)^{1/2}$). Also note that due to the specific choice of $u_{ref,1D}$, ε^2 in (2.21) and (2.22) has now to be replaced by $\frac{1}{2}$ rather than 1 in order to obtain the appropriate non-dimensional governing equations within the one-dimensional analysis.

Initial conditions within the discrete-vortex method had to be specified for the location of the fluid interfaces or the point vortices located on them, and the initial circulation of each single vortex. For a sinuousoidally disturbed liquid sheet, i.e. a sine- or cosine-disturbance imposed on the sheet, these conditions can be obtained from the linear two-dimensional analysis presented by Rangel & Sirignano (1991) and are given by

$$y^*_{i,+}|_{t^*=0} = \frac{h^*}{2} + \epsilon \sin(2\pi\xi^*_i) \quad \text{or} \quad y^*_{i,-}|_{t^*=0} = -\left[\frac{h^*}{2} + \epsilon \sin(2\pi(\xi^*_i + 0.5(k-1)))\right] \tag{3.23}$$

for the non-dimensional y-location of the ith vortex located at the upper or lower interface, and

$$\gamma^*_{i,\pm}|_{t^*=0} = \mp 2\pi\epsilon(2\pi/A)^{1/2}(A+1)\sin(2\pi\xi^*_i)/n \tag{3.24}$$

for its non-dimensional circulation. In the above equations, n is the number of point vortices per disturbance wavelength, and * denotes a non-dimensional value. The

† The two-dimensional nonlinear vortex-dynamics analysis by Rangel & Sirignano (1991) considers the general case of zero or non-zero ambient gas density which suggests the use of the relative velocity between the liquid and its surrounding gas flow U in the definition of the Weber number.

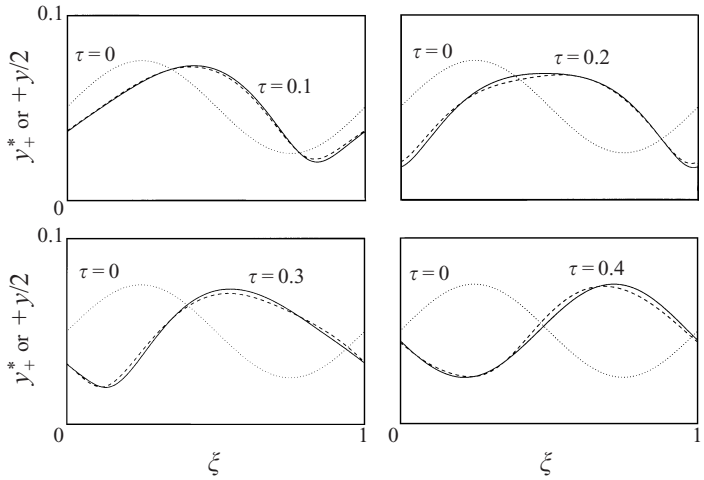

FIGURE 6. Nonlinear one-dimensional (——) and two-dimensional (— — —) solutions for the temporal evolution of a dilational travelling wave initially prescribed by (3.23) and (3.24) ($h^* = 0.1$, $\epsilon = 0.025$, $k = 1$, $A = \coth \pi h^*$).

constants k and A are given by $k = 1$ or $k = 2$ and $A = \coth(\pi h^*)$ or $A = \tanh(\pi h^*)$ for dilational or sinuous disturbances, respectively. In (3.23) and (3.24) ϵ and h^* denote the non-dimensional disturbance amplitude and thickness of the sheet, respectively. Initial conditions for the corresponding reduced-dimension simulations are to be specified for the sheet thickness y, the sheet-centreline location Y, the sheet velocity in the axial direction u and the sheet velocity in the transverse flow direction v. The initial variation of the (non-dimensional) sheet thickness y and the sheet-centreline location Y are chosen in accordance with the interface locations specified for the vortex-method simulations (3.23). The initial disturbances of the non-dimensional sheet velocities u and v which correspond to the circulation distribution specified for the two-dimensional simulations along the disturbed interface location (3.24) are obtained from the definition of the averaged (dimensional) velocities $\overline{u}(x) \equiv (1/\tilde{y}) \int_{y_-}^{y_+} v_x(x, y)\, \mathrm{d}y$ and $\overline{v}(x) \equiv (1/\tilde{y}) \int_{y_-}^{y_+} v_y(x, y)\, \mathrm{d}y$ where the local velocity components in the axial and transverse flow direction v_x and v_y are obtained from the circulation along the fluid interfaces, by using Biot-Savart's law (Schlichting & Truckenbrodt 1967). Note that $u = u_0/u_{ref}$ and $v = v_0/u_{ref}$ where $u_0(x, t)$ and $v_0(x, t)$ are the lowest-order approximations to the axial and transverse velocity components which agree with the previously defined averaged values $\overline{u}$ and $\overline{v}$ (Mehring & Sirignano 1998*a*).

Also, note once more that the specification of the above conditions as well as the subsequently presented results are based on a frame of reference which is moving with the undisturbed sheet velocity. In other words, the coordinate system employed for the comparison between one-dimensional and two-dimensional nonlinear theory uses the same Galilean transformation as already employed previously for the comparison between linear and nonlinear one-dimensional results. However, here different values for the characteristic length and velocity are used within the non-dimensionalization process, in order to simplify the comparison with the two-dimensional discrete-vortex-method simulations. Reference lengths and velocities are the same in both one- and two-dimensional simulations; this yields $1/(2\varepsilon^2) = 1$ or $We = 1$ within the one- or two-dimensional analyses, respectively.

Figure 6 illustrates the dilational deformation of a liquid sheet due to the prescribed

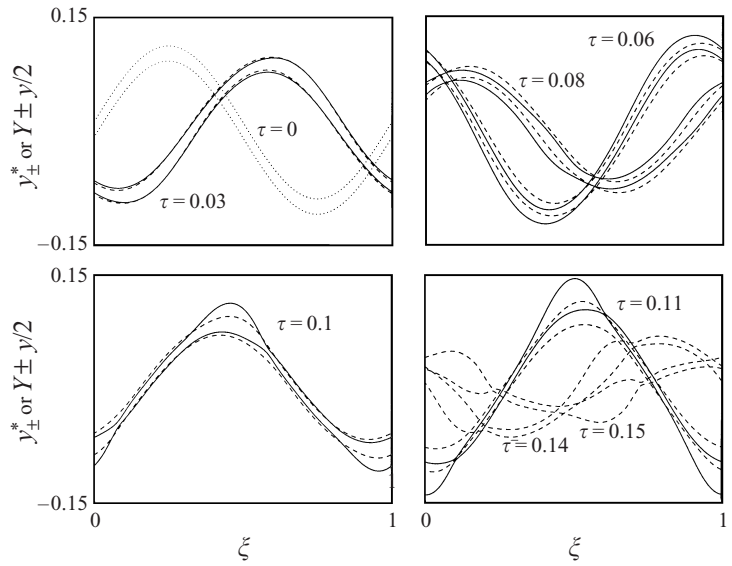

FIGURE 7. Nonlinear one-dimensional (——) and two-dimensional (— — —) solutions for the temporal evolution of a sinuous travelling wave initially prescribed by (3.23) and (3.24) ($h^* = 0.02$, $\epsilon = 0.1$, $k = 2$, $A = \tanh \pi h^*$).

initial conditions and with a non-dimensional disturbance amplitude ϵ beyond the validity limits of the linear theory ($\epsilon/h^* = 0.25$). The non-dimensional undisturbed sheet thickness for this case was chosen to be $h^* = 0.1$. From figure 6 we observe that the one-dimensional and two-dimensional simulations show the same nonlinear sheet oscillations as already analysed for the dilational case. Good agreement between one-dimensional and two-dimensional theory is found for this case. The sheet thickness of $h^* = 0.1$ here is rather large, considering our assumption of thin sheets.

Figure 7 illustrates the case of a sinuous travelling wave described by the linear initial conditions stated earlier. The non-dimensional undisturbed thickness of the sheet was $h^* = 0.02$ with the non-dimensional amplitude $\epsilon = 0.1$ for the sinuous sheet disturbance.

For the nonlinear transverse oscillation of the sheet and the agglomeration of fluid in the sheet edges as described earlier, the one-dimensional approach provides a good description of the nonlinear sinuous sheet distortion. However, in the reduced-dimension analysis the disturbance amplitude is larger than predicted by the more accurate two-dimensional simulations. Furthermore, for the case considered of an initially highly distorted and subsequently disintegrating liquid sheet, the sheet-breakup time within the one-dimensional simulations is shorter than predicted by the nonlinear two-dimensional simulations. Note however that, for very small values of h^* and ϵ/h^*, the two methods agree with each other and with the linearized one-dimensional or two-dimensional solutions (not illustrated). The simulations also showed that, as the sheet thickness h^* and/or the ratio ϵ/h^* are increased, agreement between the one-dimensional and two-dimensional approaches deteriorates for both dilational and sinuous cases; however, the reduced-dimension approach provides representative sheet dynamics even at higher values of ϵ/h^*, if the sheet thickness is not too large.

Note that, for very thin fluid sheets as they appear locally during the pinch-off in the sinuous case presented in figure 7, accurate discrete-vortex-method results are difficult to obtain at reasonable computing times; the proximity of the two interfaces

requires a high number of point vortices interspaced by a distance significantly smaller than the smallest characteristic length in the problem. For liquid sheets that are tearing, that smallest length becomes the distance between the two interfaces or the instantaneous thickness of the sheet. Also, as already mentioned in § 3.3.1, increasing numerical error during the time-integration process within the discrete-vortex method simulations will affect the accuracy of the vortex-dynamics solutions, so that comparisons with solutions from the reduced-dimension analysis cannot be performed at later times, i.e. for 'large' values of τ, if these comparisons are to be used to assess the accuracy of the simplified theory. The two-dimensional simulations presented in figures 6 and 7 were conducted by using $n = 100$ or 140 point vortices (per wavelength) at a non-dimensional integration time step of $\Delta\tau = 5 \times 10^{-5}$. The two-dimensional simulations illustrated in figure 7 have also been conducted for $n = 200$ and $\Delta\tau = 2.5 \times 10^{-5}$. Only minor differences between the two different results were observed. The reduced, one-dimensional results were obtained by using $\Delta\xi = 0.01$ or 2.5×10^{-3} and $\Delta\tau = 10^{-4}$ or 1.6×10^{-5} as non-dimensional mesh size and integration time step, respectively. Computational times required for the simulations presented were of the order of 10 CPU seconds for the one-dimensional simulations and 10^4 CPU seconds for the corresponding two-dimensional discrete-vortex-method simulations. The simulations for both one-dimensional and two-dimensional cases were conducted on a DEC-alpha workstation. The previous statements on the CPU time required for the different simulations clearly show that the reduced-dimension approach will be a valuable tool for the analysis of geometrically more complex sheet configurations, such as thin conical sheets. It is acknowledged that recently developed multi- or two-fluid methods, such as the level-set and vortex-dynamics methods, and volume-of-fluid approaches described in § 1.3 have the capability to predict such flow configurations. However, as already noted, these methods are often less accurate in the tracking of the fluid interfaces; this is particularly true for Eulerian methods using a fixed grid (Shyy *et al.* 1996). Lagrangian methods such as boundary-element or vortex-dynamics methods and some Eulerian methods which employ adaptive regridding are more accurate in the tracking of discontinuities; however, they are in general highly computationally intensive. Note that the proposed reduced-dimension analysis provides more insight to the physical problem considered than the previously mentioned more general but also more complex methods for which analytical considerations are not feasible or are very difficult to accomplish. One example of the insights developed from this method is the understanding of the nonlinear coupling between the dilational and sinuous modes that is evident through the system (2.10), (2.11), (2.17), and (2.18).

4. Semi-infinite sheets

Liquid sheets are in general generated by plane or circular slit nozzles or by diverging nozzle configurations (swirl nozzle, hollow cone; fan spray nozzle) through which the liquid is forced by a given pressure gradient. The analysis of semi-infinite sheets which are modulated/forced at the nozzle is therefore of greater practical interest than the analysis of infinitely long sheets presented earlier. The analysis presented here only considers the convective nature of waves generated at the nozzle exit.

As for the infinite case, the equations governing the nonlinear or linear distortion of semi-infinite planar liquid sheets in a void are given by (2.20)–(2.24) or (2.25)–(2.28), respectively. However, for the semi-infinite configuration a Galilean transformation

of the governing equations does not yield any simplification. This would imply the transformation of locally fixed boundary conditions at the end of the sheet to boundary conditions which are to be applied at varying locations in the transformed space. Since the undisturbed sheet velocity U is retained in this analysis, we use $l_{ref} = h$ and $u_{ref} = U$ in the non-dimensionalization process described in § 2 which then yields $\varepsilon^2 = 1/(2We)$ in (2.21), (2.22), (2.26) and (2.27), where $We = \rho U^2 h/\sigma$ is the Weber number evaluated using the thickness h and velocity U of the undisturbed sheet.† There are two characteristic velocities $v_{I,II}$ in the semi-infinite case with $1/We = 2\varepsilon^2 = v_{II}^2/v_I^2$, i.e. $v_{II} = (\sigma/\rho h)^{1/2}$ which is analogous to the characteristic velocity u_{ref} chosen in the infinite sheet analysis, and $v_I = U$ which could be omitted in the infinite case by Galilean transformation. Note that $\sqrt{2}v_{II}$ is the capillary velocity at which sinuous waves of small amplitude travel along the sheet of liquid in a manner analogous to waves on a string (Pimbley 1976).

4.1. *Linear analysis*

Using the thickness h and velocity U of the undisturbed sheet as characteristic length and velocity in the non-dimensionalization process described in § 2, we have $u^{(0)} = 1$ and $y^{(0)} = 1$ within the linearized system (2.25)–(2.28). As already stated, (2.25), (2.26) and (2.27), (2.28) are decoupled from each other so that the subsequent analysis for dilational and sinuous modulated semi-infinite sheets can be performed separately.

The linear solutions presented below illustrate the general linear behaviour of thin semi-infinite sheets with streamwise or transverse modulations enforced at the nozzle exit. It is understood that the linear solutions which involve large maximum disturbance amplitudes and/or high forcing frequencies lie beyond the validity of this linearized reduced-dimension analysis.

4.1.1. *Dilational case*

A modal analysis of (2.25) and (2.26) is conducted by assuming wave-like solutions for the non-dimensional sheet thickness $y = 1 + y'$ and sheet velocity $u = 1 + u'$ of the forms

$$y' = a\mathrm{e}^{\mathrm{i}(\omega t^* - kx^*)}, \quad u' = b\mathrm{e}^{\mathrm{i}(\omega t^* - kx^*)}, \tag{4.1}$$

where ω is the non-dimensional oscillation frequency of the sheet and $k = 2\pi/\lambda^*$ is the non-dimensional disturbance wavenumber. A similar linear analysis has already been presented by Pimbley (1976) and Bogy (1978) for semi-infinite round liquid jets. Introducing the above solutions for y and u into (2.25) and (2.26) yields the condition

$$\varepsilon^2 k^4 - (\omega - k)^2 = 0 \tag{4.2}$$

for non-trivial solutions to exist. This condition provides the dispersion relation $\omega(k) = k \pm \varepsilon k^2$, where the first term on the right-hand side is due to the non-zero propagation velocity U of the undisturbed sheet. Since ω is prescribed by the boundary conditions enforced at $x^* = 0$, we can solve for wavenumber k to yield the four roots

$$k_{1,2} = \frac{1 \pm (1 - 4\varepsilon\omega)^{1/2}}{2\varepsilon}, \quad k_{3,4} = \frac{-1 \pm (1 + 4\varepsilon\omega)^{1/2}}{2\varepsilon}, \tag{4.3}$$

where the + or – sign relates to k_1 and k_3 or k_2 and k_4, respectively. The dependence of the wavenumbers k_i on the forcing period $T = 2\pi/\omega$ is illustrated in figure 8.

† Note that the Weber number is not a characterizing/critical quantity in the consideration of the infinite sheet problem, since the undisturbed sheet velocity U (dimensional) or $u^{(0)}$ (non-dimensional) could be easily eliminated by a Galilean transformation.

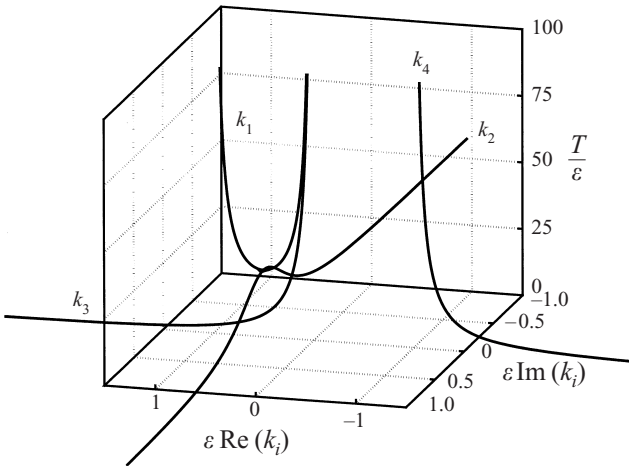

FIGURE 8. The dependence of wavenumbers k_i for modulated symmetric distorting semi-infinite sheets on forcing period $T = 2\pi/\omega$.

Note that $k_{1,2}$ can be complex, and $k_{3,4}$ are always real. Also, the solutions for k_i obtained for the case $\varepsilon \to \infty$ or $U \to 0$, i.e. $k_{1,2} = \pm \mathrm{i}(\omega/\varepsilon)^{1/2}$ and $k_{3,4} = \pm(\omega/\varepsilon)^{1/2}$, recover the linearized solutions to (3.2) for the infinite liquid sheet after Galilean transformation. Using the four solutions obtained for the wavenumbers k_i in (4.3), the general solution to (2.25) and (2.26) is given by

$$y' = \sum_{i=1}^{4} a_i \mathrm{e}^{\mathrm{i}(\omega t^* - k_i x^*)}, \quad u' = \sum_{i=1}^{4} b_i \mathrm{e}^{\mathrm{i}(\omega t^* - k_i x^*)}, \tag{4.4}$$

where the coefficients a_i and b_i are linearly dependent on each other according to equations (2.25) and (2.26). This might suggest that four boundary conditions are to be specified at $x^* = 0$; however, wavenumbers k_1 and k_2 provide a non-wave-like, exponential behaviour if the forcing of the sheet (at $x^* = 0$) is such that $\omega > 1/(4\varepsilon)$. This would imply that a modulated two-dimensional semi-infinite thin liquid sheet might be spatially unstable, whereas it is well-known that an infinite planar liquid sheet in a void and with non-zero surface tension is temporally stable by linear analysis. Although this might seem reasonable at first, we will subsequently show that this is not the case. In the spatial analysis of the semi-infinite sheet, energy is added to the system due to the time-dependent forcing at the boundary, whereas in the temporal analysis of the infinite sheet, energy is not added but only transported along the sheet.

The conservation equation for wavenumber k_i is given by Whitham (1974):

$$\frac{\partial k_i}{\partial t^*} + \frac{\partial \omega}{\partial x^*} = 0 \quad \text{or} \quad \frac{\partial k_i}{\partial t^*} + C(k_i)\frac{\partial k_i}{\partial x^*} = 0, \tag{4.5}$$

where $C(k_i) = \mathrm{d}\omega/\mathrm{d}k_i$ denotes the group velocity of wavenumber k_i obtained from the dispersion relation $\omega(k_i)$,

$$C(k_{2,3}) = +(1 \mp 4\varepsilon\omega)^{1/2} \quad \text{or} \quad C(k_{1,4}) = -(1 \mp 4\varepsilon\omega)^{1/2}. \tag{4.6}$$

Therefore, on an initially undisturbed sheet, wavenumbers k_1 and k_4 will appear only upstream and k_2 and k_3 will appear only downstream from the location where some disturbance is forced onto the moving sheet. See figure 9. This is analogous to the

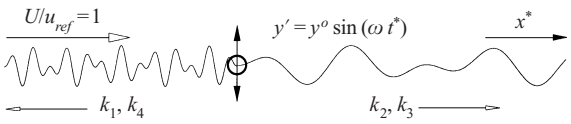

FIGURE 9. Wave propagation on a fluid sheet initiated by a local disturbance.

appearance of gravity waves and capillary waves, downstream and upstream of an obstacle on the surface of a liquid stream (Whitham 1974).

Similarly, on a semi-infinite sheet subject to disturbances of some frequency ω at an orifice (located at $x^* = 0$), only wavenumbers k_2 and k_3 will appear at $x^* > 0$. This implies that the roots k_1 and k_4 have to be excluded from the solution for $x^* > 0$, such that y' or u' do not exponentially grow as $x^* \to \infty$ for any value of ω. In other words, the semi-infinite sheet is unconditionally stable by linear analysis. Since there are only two remaining roots k_2 and k_3, only two boundary conditions should be specified at $x^* = 0$, in order to determine the fluctuations of sheet thickness $y'(x^* > 0, t^*)$ and velocity $u'(x^* > 0, t^*)$, i.e. $y'_{2,3} = a_{2,3}\,\mathrm{e}^{\mathrm{i}(\omega t^* - k_{2,3}x^*)}$ and $u'_{2,3} = b_{2,3}\,\mathrm{e}^{\mathrm{i}(\omega t^* - k_{2,3}x^*)}$.

The notion of a meaningful group velocity $C(k_{1,2}) = \mathrm{d}\omega/\mathrm{d}k_{1,2}$ only applies for cases where k_1 and k_2 are real, i.e. $\omega < 1/(4\varepsilon)$. For $\omega > 1/(4\varepsilon)$, $C(k_{1,2})$ is given by $C(k_{1,2}) = \mathrm{d}\omega/\mathrm{d}\,[Re(k_{1,2})]$. For the k_1 or k_2 branch, the group velocity has positive or negative infinite values if the wavenumber is complex. Within the present analysis it is assumed that, if k_1 and k_2 become complex as ω changes, the direction of propagation of information is the same as it was in the neighbouring region where both wavenumbers were real. This implies that k_1 (with its negative group velocity) is to be disregarded for any forcing frequency ω and k_2 (with its positive group velocity) is to be included in the analysis for any ω. The same result would have been obtained by following the assumption to disregard a certain root k_i for all values of ω, if it is to be disregarded at some value ω. This assumption is generally more restrictive and has been employed by Bogy (1978) in his linear analysis of semi-infinite round liquid jets. However, the difference between the two approaches is not manifested in the planar case.

The demonstrated use of group velocity arguments in order to determine where waves will appear is closely related to energy-transport considerations employing the Sommerfeld radiation condition (Whitham 1974). In the present problem, this implies that the energy transport along the sheet is outgoing as $x^* \to \infty$; in other words, energy cannot travel upstream from infinity (Bogy 1978). Since the group velocity $C(k)$ is related to energy propagation (Whitham 1974; Bogy 1978), wavenumbers k_1 and k_4 are then excluded in determining $u'(x^* > 0, t^*)$ and $y'(x^* > 0, t^*)$. In this sense, the Sommerfeld radiation condition provides two 'boundary conditions' for $x^* \to \infty$ by excluding the wavenumbers with negative group velocities. The solution is obtained by specifying two conditions at $x^* = 0$ relating to wavenumbers k_2 and k_3. The exclusion of certain wavenumbers k_i by using energy-transport arguments has already been illustrated (Bogy 1978). Also, the above considerations about the appearance of certain wavenumbers downstream from the nozzle and the specification of appropriate boundary conditions at the nozzle are in agreement with numerical simulations of the corresponding dilational transient problem (§ 4.2.1). The same is true for the similar considerations employed for sinuous or antisymmetric modulated sheets (§ 4.1.2, § 4.2.2).

The linearized semi-infinite sheet problem for dilational disturbances as described above has been solved by using $y'(x^* = 0, t^*) = 0$ and $u'(x^* = 0, t^*) = u^o\mathrm{e}^{\mathrm{i}\omega t^*}$ as

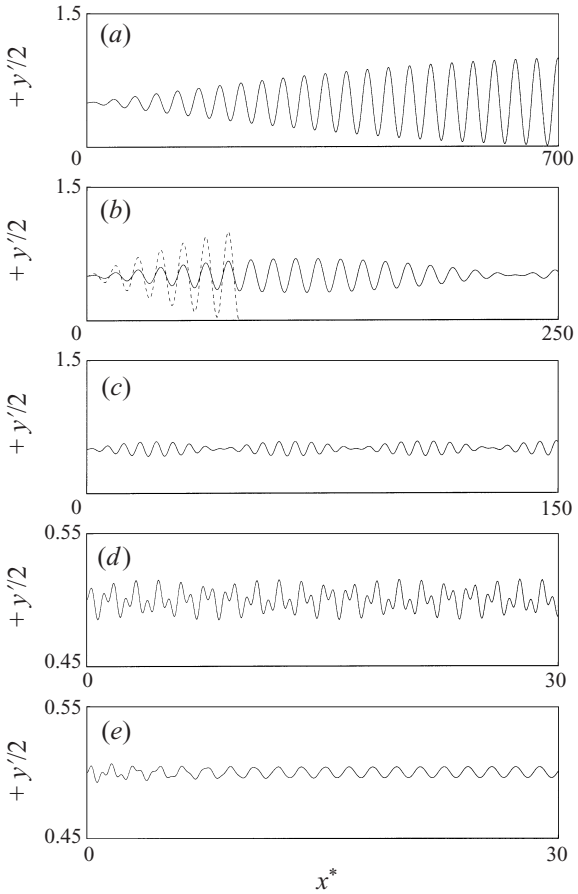

FIGURE 10. Time-periodic solution ($t^* = n\,T, n \in \mathrm{I}$) to the linear boundary value problem given by a semi-infinite planar sheet with harmonic dilational forcing at $x^* = 0$ (forcing frequency $\omega = 2\pi/T$, $\varepsilon = (2We)^{-1/2} = 0.05$, $A_{y'} = 0$). (*a*) $\omega = 0.2$, $A_{u'} = 0.01$, $k_2 = 0.202$, $k_3 = 0.198$; (*b*) $\omega = 0.525$, $A_{u'} = 0.01$ (——) or 0.03 (– – –), $k_2 = 0.54$, $k_3 = 0.512$; (*c*) $\omega = 1.2$, $A_{u'} = 0.01$, $k_2 = 1.282$, $k_3 = 1.136$; (*d*) $\omega = 4.95$, $A_{u'} = 0.01$, $k_2 = 9$, $k_3 = 4.108$; (*e*) $\omega = 5.0025$, $A_{u'} = 0.01$, $k_2 = 10 - \mathrm{i}\,0.022$, $k_3 = 4.144$.

boundary conditions imposed at $x^* = 0$ where the sheet exits the nozzle or atomizer. The flow is in the positive x^*-direction for $0 \leqslant x^* \leqslant \infty$. Similar conditions were employed by Meier *et al.* (1992) in their experimental investigation of circular jets, which also included theoretical analyses for both circular and planar semi-infinite liquid streams. The corresponding time-dependent solution for $y'(x^* > 0, t^*)$ is given by

$$y'(x^*, t^*) = \frac{u^o k_2 k_3}{\omega(k_3 - k_2)} \left[\mathrm{e}^{\mathrm{i}\,(\omega t^* - k_2 x^*)} - \mathrm{e}^{\mathrm{i}(\omega t^* - k_3 x^*)}\right], \tag{4.7}$$

where the wavenumbers $k_{2,3}(\omega, \varepsilon)$ are given by (4.3). Note that the amplitude $u^o k_2 k_3/(\omega(k_3 - k_2))$ in (4.7) is real if $\omega < 1/(4\varepsilon)$ but complex if $\omega > 1/(4\varepsilon)$, assuming u^o is real. Figure 10(*a–e*) shows the real part of this solution, corresponding to a harmonic forcing of the sheet velocity by $\mathrm{Re}(u') = A_{u'} \cos(\omega t^*)$ at $x^* = 0$ as already stated.

Figure 10(*a–e*) refers to a high-velocity jet or a high Weber number case ($(2We)^{-1/2} = \varepsilon = 0.05$). The velocity disturbance imposed on the liquid sheet is characterized by

its amplitude $A_{u'} = 0.01$ or 0.03 and its forcing frequency $\omega = 0.2$, 0.525, 1.2, 4.95 or 5.0025. Two of these cases ($A_{u'} = 0.01$ and $\omega = 0.525$ or 1.2) parallel cases considered by Pimbley (1976) and Bogy (1978) for a circular liquid jet. From (4.3) and (4.7) we see that, for small ω, k_2 and k_3 are only slightly different, providing two constant-amplitude waves of nearly equal wavelength propagating at different phase speeds. One is slightly slower and the other is slightly faster than the jet, so that the disturbance amplitude of the sheet thickness takes the form of a long-wavelength envelope of a short-wavelength oscillation. Equation (4.7) also illustrates that, as k_2 and k_3 approach the same value, the maximum amplitude of this envelope increases which ultimately leads to a breakup of the sheet if the maximum disturbance amplitude is greater than or equal to the value of the undisturbed sheet thickness (figure 10*a*). At higher forcing frequencies but same forcing amplitude $A_{u'}$, the wavelength of this envelope decreases, the overall thinning of the sheet is smaller and sheet breakup does not occur (figure 10*b–e*). However, as $A_{u'}$ is increased the sheet might also break up at these higher forcing frequencies (figure 10*b*), due to the linear increase of the disturbance amplitude with $A_{u'}$ or u^o according to (4.7). The breakup length is decreased as $A_{u'}$ is increased. Figure 10(*d*) also shows that at higher values of ω, k_2 and k_3 take significantly different values, such that the solution does not appear to be harmonic any more. As ω takes values greater than $\omega_{cr} = 1/(4\varepsilon)$, k_2 becomes complex resulting in a sheet distortion which involves an exponentially decaying periodic contribution as illustrated in figure 10(*e*).

As the Weber number of the sheet is lowered, k_2 and k_3 change such that the amplitude of the resulting envelope is decreased (not illustrated). This result is directly obtained by investigating the dependence of the solution (4.7) on ε. In fact, combining (4.3) with (4.7) shows that the maximum amplitude of the linear sheet distortion is a function of u^o and ($\varepsilon\omega$) only. The amplitude monotonically decreases with increasing magnitude of the product ($\varepsilon\omega$). As already stated, it also decreases linearly with decreasing amplitude of the imposed velocity disturbance u^o or $A_{u'}$. This is true for any value of ω, even though k_2 and therefore the amplitude $u^o k_2 k_3/(\omega(k_3 - k_2))$ in (4.7) might be complex for high values of ω. In that sense, a lower jet velocity or higher surface-tension coefficient (i.e. lower Weber number) is stabilizing on a semi-infinite liquid sheet with a velocity disturbance forced at one end. This is in contrast to the results obtained by Pimbley (1976) and Bogy (1978) for semi-infinite circular jets, where an increase in surface tension or decrease in jet velocity is destabilizing due to the radius of curvature in the circumferential direction.

4.1.2. *Sinuous case*

Analogous to the previous analysis of semi-infinite dilational distorting sheets, solutions to (2.27) and (2.28) are sought by modal analysis. Solutions for Y' and v' are assumed to be of the form

$$Y' = c\,\mathrm{e}^{\mathrm{i}(lx^* - \omega t^*)}, \quad v' = d\,\mathrm{e}^{\mathrm{i}(lx^* - \omega t^*)}, \tag{4.8}$$

where l and ω denote the non-dimensional disturbance wavenumber $2\pi/\lambda^*$ and the non-dimensional transverse oscillation frequency enforced at the nozzle exit. Introducing these solutions into (2.27) and (2.28) yields the condition

$$\omega = l \pm 2\varepsilon l \tag{4.9}$$

for non-trivial solutions to exist. Equation (4.9) differs significantly from the corresponding relation (4.2) derived for dilational waves. It predicts that the propagation velocity $V^* = \omega/l = 1 \pm 2\varepsilon$ is the same for all sinuous travelling waves; there is no

wave dispersion as predicted for dilational waves. The same observation was made in § 3.1 for periodically disturbed infinite sheets.

Analogously to the dilational analysis of the previous section (§ 4.1.1), (4.9) is solved for wavenumber l, since the transverse oscillation frequency ω is prescribed by the boundary conditions enforced at the nozzle exit (at $x^* = 0$). This yields the two real solutions

$$l_{1,2} = \frac{\omega}{1 \pm 2\varepsilon}. \tag{4.10}$$

Note that, as $\varepsilon \to \infty$ or $U \to 0$, one obtains $l_{1,2} = \pm\omega/(2\varepsilon)$ which yields the solutions to (3.3) for infinite sinuous distorting sheets in a reference frame moving with the undisturbed sheet velocity. From (4.8) and (4.10) the general solution to (2.27) and (2.28) is found, i.e.

$$Y' = \sum_{i=1}^{2} c_i \mathrm{e}^{\mathrm{i}(l_i x^* - \omega t^*)}, \quad v' = \sum_{i=1}^{2} d_i \mathrm{e}^{\mathrm{i}(l_i x^* - \omega t^*)}, \tag{4.11}$$

with $l_{1,2}$ given by (4.10), and c_i and d_i being related by (2.28), i.e. $d_i = \mathrm{i}(l - \omega)c_i$. The latter implies that no more than two of these coefficients may be chosen independently. This is observed more readily by reducing (2.27) and (2.28) to a single equation governing $Y'(x^*, t^*)$. The general solution to this equation is then given by (4.11) for Y' with the free coefficients $c_{1,2}$ and $l_{1,2}$ provided by (4.10).

As for dilational waves on semi-infinite fluid sheets, group velocity arguments can now be used to determine which waves generated by the transverse sheet oscillation enforced at the nozzle exit ($x^* = 0$) will appear downstream at $x^* > 0$.

From (4.9), the group velocities $C(l_i) = \mathrm{d}\omega/\mathrm{d}l_i$ for the two waves with wavenumbers l_1 and l_2 are the same as their corresponding wave velocities, i.e.

$$C(l_{1,2}) = 1 \pm 2\varepsilon. \tag{4.12}$$

Equation (4.12) shows that both waves will appear on the semi-infinite sheet ($0 \geqslant x^* \geqslant \infty$) as long as $\varepsilon < 1/2$ or $We > 2$. However, for cases where the Weber number We has values below 2, only the wave with wavenumber $l_1 = \omega/(1 + 2\varepsilon)$ is expected to appear at downstream locations $x^* > 0$. Accordingly, two boundary conditions are to be prescribed at $x^* = 0$ if $We > 2$, but only one condition may be imposed at the nozzle exit for cases where $We < 2$. For the former case (i.e. $We > 2$), the linearized semi-infinite sheet problem for sinuous disturbances has been solved by using $Y'(x^* = 0, t^*) = Y^o \mathrm{e}^{-\mathrm{i}\omega t^*}$ and $v'(x^* = 0, t^*) = v^o \mathrm{e}^{-\mathrm{i}\omega t^*}$ as boundary conditions imposed at $x^* = 0$. (Note that, Y^o and v^o might be complex.) The corresponding time-dependent solution for $Y'(x^* > 0, t^*)$ is given by

$$Y'(x^*, t^*) = \frac{Y^o(\omega - l_2) - \mathrm{i}\, v^o}{l_1 - l_2} \mathrm{e}^{\mathrm{i}(l_1 x^* - \omega t^*)} + \frac{Y^o(\omega - l_1) - \mathrm{i}\, v^o}{l_2 - l_1} \mathrm{e}^{\mathrm{i}(l_2 x^* - \omega t^*)}. \tag{4.13}$$

We observe that the maximum amplitude of the sheet disturbance $Y'(x^*, t^*)$ depends linearly on the values of the forcing amplitudes Y^o and v^o, and increases as l_1 and l_2 approach the same value ω for $\varepsilon \to 0$.† The latter also implies that the sheet distortion for low values of ε is characterized by a long-wavelength envelope of a short-wavelength oscillation. Equation (4.13) also illustrates that the maximum disturbance amplitude is influenced by the phase angle between the harmonic disturbances forced

† As ε is varied from 0 to $\frac{1}{2}$, the non-dimensional wavenumber l_1 decreases from ω to $\omega/2$, whereas l_2 increases from ω to infinity. This corresponds to an increase in wavelength $\lambda_1 = 2\pi/l_1$ from $2\pi/\omega$ to $4\pi/\omega$, or a decrease in $\lambda_2 = 2\pi/l_2$ from $2\pi/\omega$ to 0.

onto Y' and v'. Further details on the solution presented in (4.13) can be obtained by substituting $l_{1,2}$ from (4.10) into (4.13). Doing so, one observes that the maximum amplitude of the sinuous sheet disturbance caused by the harmonic forcing of the transverse velocity v' decreases with an increase in the forcing frequency ω or a decrease of the Weber number $We = 1/(2\varepsilon^2)$. However, the amplitude disturbance caused by harmonic variations of Y' at $x^* = 0$ does not depend on the frequency of this variation. For a harmonic forcing of the sheet centreline Y' at the nozzle exit, increasing values of ε (corresponding to a decrease in Weber number We) causes an increase in the sheet-disturbance amplitude of the longer wave (wavenumber l_1) but a decrease in the amplitude of the shorter wave (wavenumber l_2). As ε is increased from zero (zero-surface-tension case) to $1/2$ (maximum ε value for which both waves appear at $x^* > 0$) the wave amplitude corresponding to l_1 varies between $Y^o/2$ and Y^o, and the amplitude for the wave with wavenumber l_2 changes from Y^o to zero. Note that, for a harmonic forcing of v' at $x^* = 0$, the maximum wave amplitude approaches infinity as $\varepsilon \to 0$.

Figure 11(*a–e*) illustrates the sinuous distorting sheet for two different values of ε but the same frequency $\omega = 0.25$ at which the sheet centreline Y' and the transverse sheet velocity v' are forced at the nozzle exit. A phase angle of $\pi/2$ was chosen between the harmonic forcing of Y' and v', i.e.

$$Y' = A_{Y'} \sin(\omega t^*) \quad \text{and} \quad v' = A_{v'} \cos(\omega t^*) \tag{4.14}$$

was assumed. For the illustrated cases, the (real) forcing amplitudes were chosen among $A_{Y'} = 0, 0.2$ and $A_{v'} = 0, 0.005, 0.05$. The corresponding (linear) solutions are given by the imaginary part of the solution (4.13) with $Y^o = -A_{Y'}$ and $v^o = \mathrm{i}\, A_{v'}$.

Figure 11(*a–e*) demonstrates that the wavelength of the observed sheet envelope increases as $\varepsilon = (2We)^{-1/2}$ is decreased. From the cases with $A_{Y'} = 0$ we also observe that the maximum disturbance amplitude increases with a decrease in ε or an increase in $A_{v'}$. For the case with $\varepsilon = 0.05$ and transverse velocity disturbance only ($A_{v'} = 0.005$), the result resembles figure 10(*c*) for the dilational case. Also note that, for $\varepsilon = 0.05$ with $A_{Y'} = 0.2$ and $A_{v'} = 0.005$ simultaneously, the beat amplitude of the resulting linear solution is virtually zero (not illustrated). However, under the same forcing conditions but with a different ε-value ($\varepsilon = 0.02$), the beat behaviour is still observed. (See figure 11*e*.) The characteristic beat in the sinuous distortion of semi-infinite sheets was also observed experimentally by Hashimoto & Suzuki (1991).

When $We < 2$, only one wave travels downstream from the nozzle exit. Therefore, a sinusoidal forcing at the exit results in a constant-amplitude wave travelling downstream according to the linear solution.

Finally, it should be noted once more that, in contrast to the dilational distortion of semi-infinite sheets, ω does not influence the ratio between wavenumbers l_1 and l_2, but merely their absolute values and the disturbance amplitude of Y' caused by the harmonic forcing of v' at $x^* = 0$. Also, by linear analysis, harmonic disturbances of v' and/or Y' only will not cause the sheet to break up at a finite time. This is in contrast to the linear results presented earlier for dilational disturbances imposed on the sheet at the nozzle exit. However, as described below, sinuous distorting sheets might break up due to nonlinear effects.

4.2. *Nonlinear numerical analysis*

The equations governing the nonlinear symmetric or antisymmetric distortion of a thin inviscid semi-infinite planar liquid sheet in a void with time-dependent forcing at one end have been solved numerically. Solutions were obtained explicitly by using

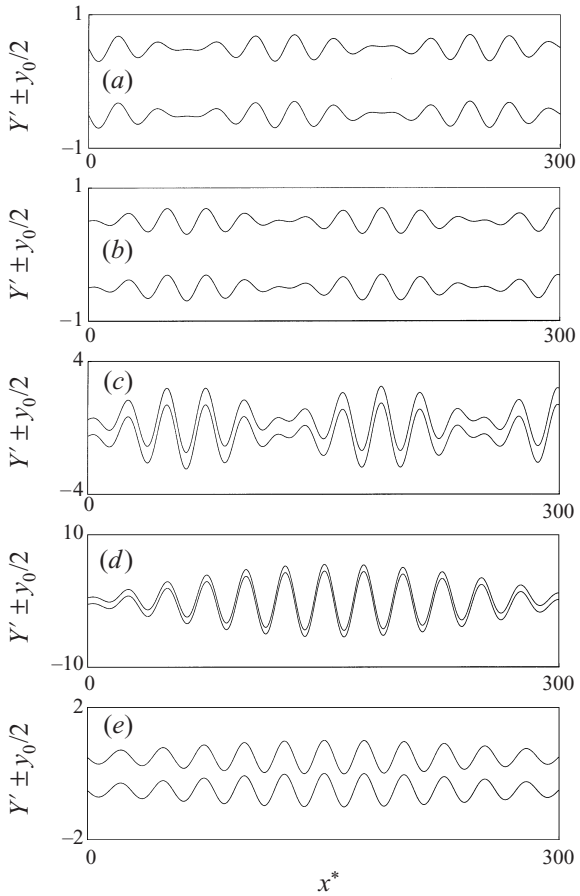

FIGURE 11. Time-periodic solution ($t^* = nT, n \in \mathrm{I}$) to the linear boundary value problem given by a semi-infinite planar sheet with harmonic sinuous forcing at $x^* = 0$ (forcing frequency $\omega = 2\pi/T = 0.25$). (*a*) $\varepsilon = 0.05$, $A_{Y'} = 0.2$, $A_{v'} = 0$, $l_1 = 0.227$, $l_2 = 0.278$; (*b*) $\varepsilon = 0.05$, $A_{Y'} = 0$, $A_{v'} = 0.005$, $l_1 = 0.227$, $l_2 = 0.278$; (*c*) $\varepsilon = 0.05$, $A_{Y'} = 0$, $A_{v'} = 0.05$, $l_1 = 0.227$, $l_2 = 0.278$; (*d*) $\varepsilon = 0.02$, $A_{Y'} = 0$, $A_{v'} = 0.05$, $l_1 = 0.24$, $l_2 = 0.26$; (*e*) $\varepsilon = 0.02$, $A_{Y'} = 0.2$, $A_{v'} = 0.005$, $l_1 = 0.24$, $l_2 = 0.26$.

the same numerical scheme as employed for periodically disturbed infinite sheets, i.e. the Lax–Wendroff method with Richtmyer splitting, and/or the 'angled-derivative' scheme described by Richtmyer & Morton (1967).

4.2.1. *Dilational case*

For modulated, symmetric distorting semi-infinite sheets, the same time-dependent boundary conditions were specified at $x^* = 0$ as in the corresponding linear case. However, a phase shift of $\pi/2$ was employed in order to reduce oscillations in the solution, which are produced as the disturbances generated at the nozzle exit start propagating downstream, into the undisturbed sheet. The specification of an additional condition at this boundary was needed within the numerical schemes employed, in order to evaluate the highest-order spatial derivative of y near the boundary. Only minor differences in the numerical solutions were found when specifying different higher-order spatial derivatives in y for this additional condition (i.e. $\partial^n y/\partial x^{*n}$; $n = 4, 5$). For the results presented below, $(\partial^4 y/\partial x^{*4})_{x^*=0} = 0$ has been used. For this case, the two nu-

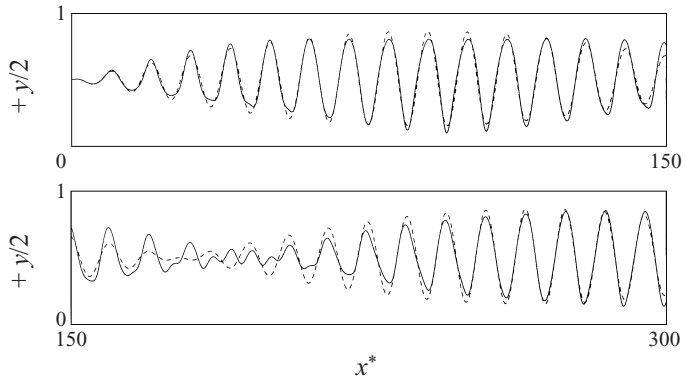

FIGURE 12. Dilational distortion of a semi-infinite planar liquid sheet at time $t^* = 35T$. The sheet is harmonically forced at $x^* = 0$ with forcing frequency ω ($A_{u'} = 0.02$, $We = 1/(2\varepsilon^2) = 250$, $T = 2\pi/\omega = 10$: – – –, linear limit cycle ($t^* = n\,T$, $n \in \mathrm{I}$); ——, nonlinear transient).

merical schemes employed were found to yield solutions which agree with each other over the considered range of Weber numbers, disturbance amplitudes and forcing frequencies. A detailed analysis on the stability of the numerical boundary condition imposed at $x^* = 0$ has not been conducted. For the simpler, one-dimensional linear convection equation, such considerations have been presented by Trefethen (1984). When using the 'angled-derivative' scheme, stability problems were encountered if $(\partial^5 y/\partial x^{*5})_{x^*=0} = 0$ was specified as numerical boundary condition.

In order to model the semi-infinite sheet properly, the boundaries of the computational domain were chosen such that the shortest resolved waves did not reach the downstream boundary within the simulation time. For the computations, an initially undisturbed sheet was assumed. In other words, the numerical models solve an initial-value and boundary-value problem, whereas the linear analysis presented above solves the boundary value problem of a semi-infinite sheet. The nonlinear oscillation does not extend to infinity in a finite time while the linear oscillation has already extended to infinity at the starting time.

The numerical schemes employed have been tested by simulating the linearized case (with the same boundary conditions) and subsequent comparison with the analytical solution. Good agreement was obtained for various forcing frequencies $\omega = 2\pi/T$ and Weber numbers above and below the critical value $We_{cr,d} = 8\omega^2$. In all cases considered, transient effects were propagated away from the nozzle at a finite time and did not prevent the development of the limit-cycle solution. The solutions illustrated below were obtained by using the 'angled-derivative' scheme and $(\partial^4 y/\partial x^{*4})_{x^*=0} = 0$ as the numerical boundary condition as already mentioned.

Figures 12 and 13 compare nonlinear numerical and linear analytical results for $We = 1/(2\varepsilon^2) = 250, 500$; $T = 2\pi/\omega = 10, 25$ and $A_{u'} = 0.02$ or 0.05. Figure 12 shows the deformed sheet at $t^* = 35T$ and illustrates that the nonlinearity does not alter the major characteristics of the sheet distortion as predicted by the linear analysis. The envelope and its maximum amplitude observed in the nonlinear simulations are well predicted by the linear analysis. However, in the nonlinear case additional higher-harmonic components are observed as the sheet propagates downstream. These higher harmonics persist on the sheet even when the disturbance front has travelled far downstream along the undisturbed sheet. Note that we compare linear solutions that

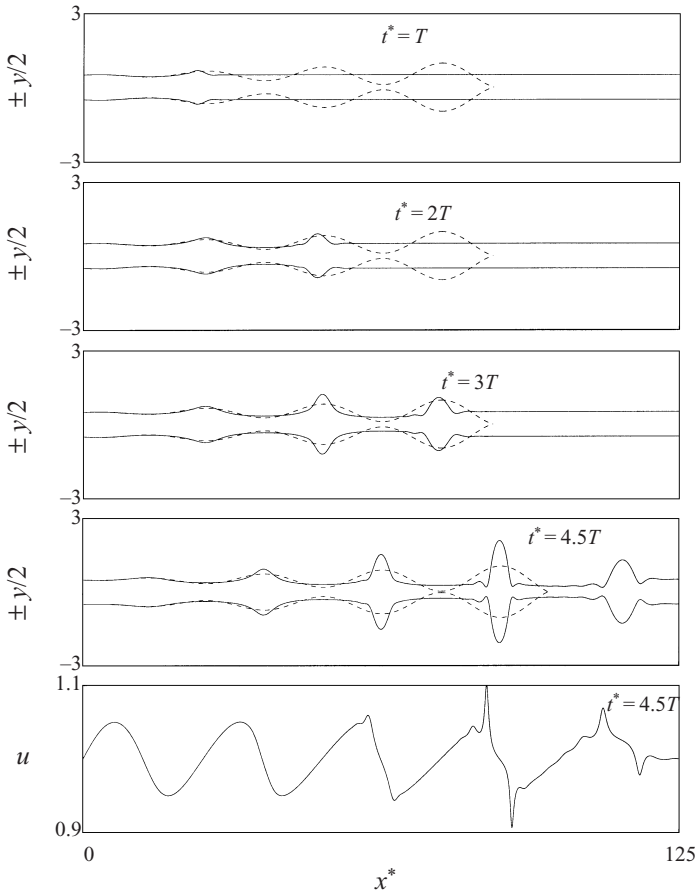

FIGURE 13. Dilational distortion of a semi-infinite planar liquid sheet harmonically forced at $x^* = 0$ with forcing frequency ω ($A_{u'} = 0.05$, $We = 1/(2\varepsilon^2) = 500$, $T = 2\pi/\omega = 25$: – – –, linear limit cycle ($t^* = n\,T$, $n \in \mathrm{I}$); ——, nonlinear transient).

have evolved after a long time to a time-periodic form with the nonlinear solutions of an initial-value problem. This is more evident in figure 13.

Figure 13 illustrates a similar case as in figure 12, but for a higher Weber number (i.e. lower surface tension), a lower forcing frequency $\omega = 2\pi/T$ and a higher amplitude $A_{u'}$ of the imposed velocity disturbance. This subsequently leads to a breakup of the sheet due to thinning. In the nonlinear case, fluid is accumulating into fluid lumps interspaced by one wavelength and connected by fluid threads. Increased sheet thinning followed by sheet pinch-off is found to occur near the larger ligaments or fluid lumps. However, figure 13 also shows that the corresponding breakup length of the sheet predicted by linear theory is only slightly shorter than that predicted by the nonlinear simulations. The nonlinear numerical solutions presented in figures 12 and 13 were obtained by using $\Delta t^* = 0.0125$ and $\Delta x^* = 0.0625$ as non-dimensional time step and mesh size, respectively.

Figures 14 and 15 illustrate the dilational sheet distortion for two cases with low Weber numbers, one slightly above and the other slightly below the critical value $We_{cr,d} = 8\omega^2 \approx 0.5$ corresponding to $T = 2\pi/\omega = 25$.

Although the axial momentum disturbance imposed onto the sheet is higher in

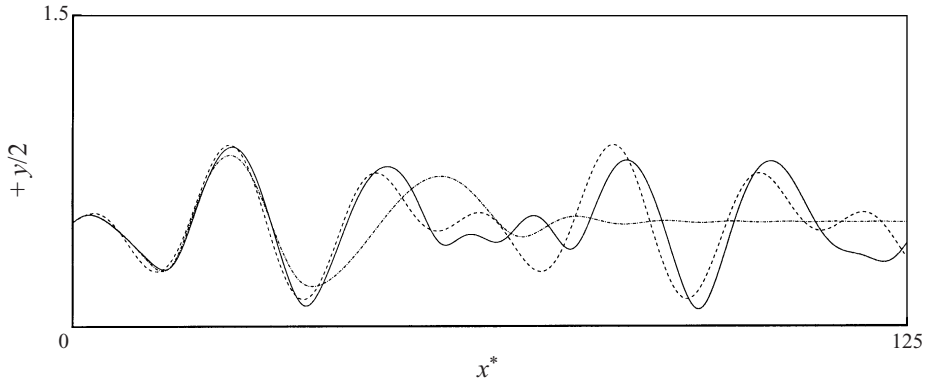

FIGURE 14. Dilational distortion of a semi-infinite planar liquid sheet harmonically forced at $x^* = 0$ with forcing frequency ω ($A_{u'} = 0.15$, $We = 1/(2\varepsilon^2) = 1$, $T = 2\pi/\omega = 25$; linear limit cycle: – – –, $t^* = n\,T$ ($n \in$ I); nonlinear transient: – · – ·, $t^* = 2T$; ——, $t^* = 8T$).

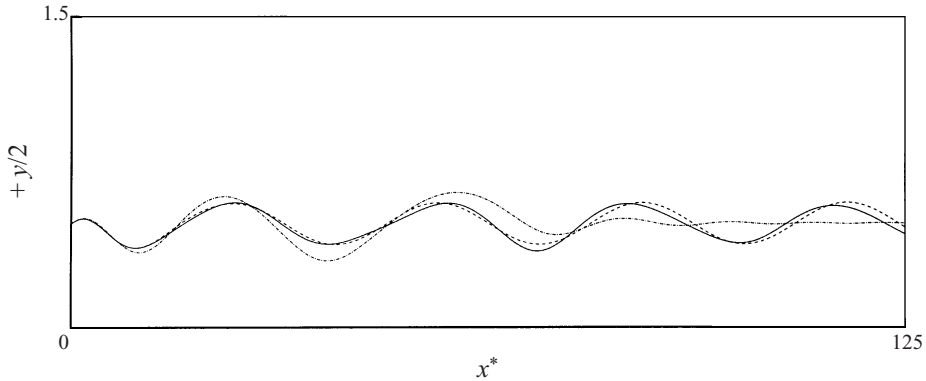

FIGURE 15. Dilational distortion of a semi-infinite planar liquid sheet harmonically forced at $x^* = 0$ with forcing frequency ω ($A_{u'} = 0.15$, $We = 1/(2\varepsilon^2) = 0.4 < We_{cr,d}$, $T = 2\pi/\omega = 25$; linear limit cycle: – – –, $t^* = n\,T$ ($n \in$ I); nonlinear transient: – · – ·, $t^* = 2T$; ——, $t^* = 8T$).

these cases (i.e. $A_{u'} = 0.15$), the relatively higher surface tension (i.e. lower Weber number) now prevents the sheet from breaking up with a decrease in the maximum disturbance amplitude of the sheet for decreasing Weber number values. For the case illustrated in figure 14, the lower Weber number ($We = 1$) results in a beat with a significantly shorter wavelength than the one associated with the case illustrated in figure 13. For the case shown in figure 15, the Weber number is 0.4 and below the critical value $We_{cr,d}$ such that, in agreement with linear theory, the numerical solution does no longer show the characteristic beat behaviour. Also note that, as the maximum disturbance amplitude decreases, agreement between the linear analytical and nonlinear numerical solutions improves. The nonlinear simulations illustrated in figures 14 and 15 employed $\Delta t^* = 6.7 \times 10^{-3}$ and $\Delta x^* = 0.2$ or 0.375, respectively. As for all the simulations presented in this paper, accuracy of the numerical solutions was demonstrated by successive refinement of mesh size and/or time step.

A nonlinear analytical solution for modulated semi-infinite symmetric distorting planar sheets such as those described above was given by Meier *et al.* (1992). However, in their analysis which did not consider surface-tension effects, the details described

(e.g. sheet thinning and breakup near fluid lumps, and characteristic beat of the distorting sheets) could not be identified.

4.2.2. *Sinuous case*

For the case of sinuous distorting semi-infinite liquid sheets in a void, with time-dependent forcing at the nozzle and $We > 2$, time-dependent boundary conditions were specified for Y and v according to those employed for the corresponding linear case discussed earlier (recall that, $Y' = Y$ and $v' = v$ in the linear sinuous case). As for the axial velocity component $u(x^* = 0, t^*)$ in the dilational case, a phase shift of $\pi/2$ was employed within the specification of $v(x^* = 0, t^*)$ in order to reduce oscillations generated in combination with the initial conditions employed, i.e. $y(x^*, t^* = 0) = u(x^*, t^* = 0) = 1$ and $Y(x^*, t^* = 0) = v(x^*, t^* = 0) = 0$. For $We < 2$ only one boundary condition, i.e. a harmonic forcing of Y given by (4.14), was specified at $x^* = 0$ in accordance with linear theory. For both cases, i.e. $We > 2$ and $We < 2$, the non-dimensional sheet velocity u and the non-dimensional sheet thickness y at the nozzle were assumed to take their undisturbed values, i.e. $u = y = 1$, at all times. Furthermore, the same numerical boundary condition was employed as in the dilational case considered previously, i.e. $(\partial^4 y/\partial x^{*4})_{x^*=0} = 0$. Also $(\partial^4 Y/\partial x^{*4})_{x^*=0} = 0$ was specified as a numerical boundary condition in order to model appropriately the highest-order spatial derivative of Y near the boundary. For the simulations illustrated below the 'angled-derivative' scheme was used. The integration time step for all the simulations was $\Delta t^* = 0.025$ with mesh sizes ranging from $\Delta x^* = 0.05$ to 0.17. For all the cases considered, the right-hand boundary of the computational domain was not reached by any sheet disturbance within the simulation time. Also, as in the dilational case, comparison between linear analytical and linear numerical solutions showed that transient effects do not influence the long-time behaviour near the nozzle or the development of the limit-cycle solution. This is not necessarily true for thin annular sheets. In fact, the authors have recently observed that, for modulated sinuous distorting annular sheets as considered by Mehring & Sirignano (1998*b*), transient effects might lead to the development of a temporal instability on the sheet. See also Lighthill (1965) in this context.

Figure 16 compares nonlinear numerical and linear analytical results for a case with high forcing amplitude of the transverse sheet velocity v at the nozzle exit, i.e. $A_{v'} = 0.05$. The forcing amplitude of the sheet centreline location Y at $x^* = 0$ was assumed to be zero. The Weber number for this case is $We = 1/(2\varepsilon^2) = 1000$ and the non-dimensional time period of the harmonic forcing is $T = 2\pi/\omega = 25$. As already noted within the analysis for dilational disturbed sheets, the linear solutions presented here and in the previous section are solutions to a pure boundary-value problem, while the corresponding nonlinear numerical solutions are the solutions to an initial- and boundary-value problem.

Comparison between the linear limit-cycle solution and the nonlinear transient solution in figure 16 shows that nonlinear effects become important as the disturbance amplitude of the sheet grows in the downstream direction. As in the infinite sinuous case analysed earlier, in the nonlinear case the sheet takes a sawtooth-like shape with fluid agglomerating in its edges. This phenomenon was also observed by Asare *et al.* (1981) in their experimental study on planar sheets modulated at the nozzle exit. Also, similar to the observation made already for infinite sinuous distorting sheets, figure 16 shows increased sheet thinning eventually leading to sheet pinch-off at points interspaced by half a wavelength and located close to the maximum deflection region of the sheet.

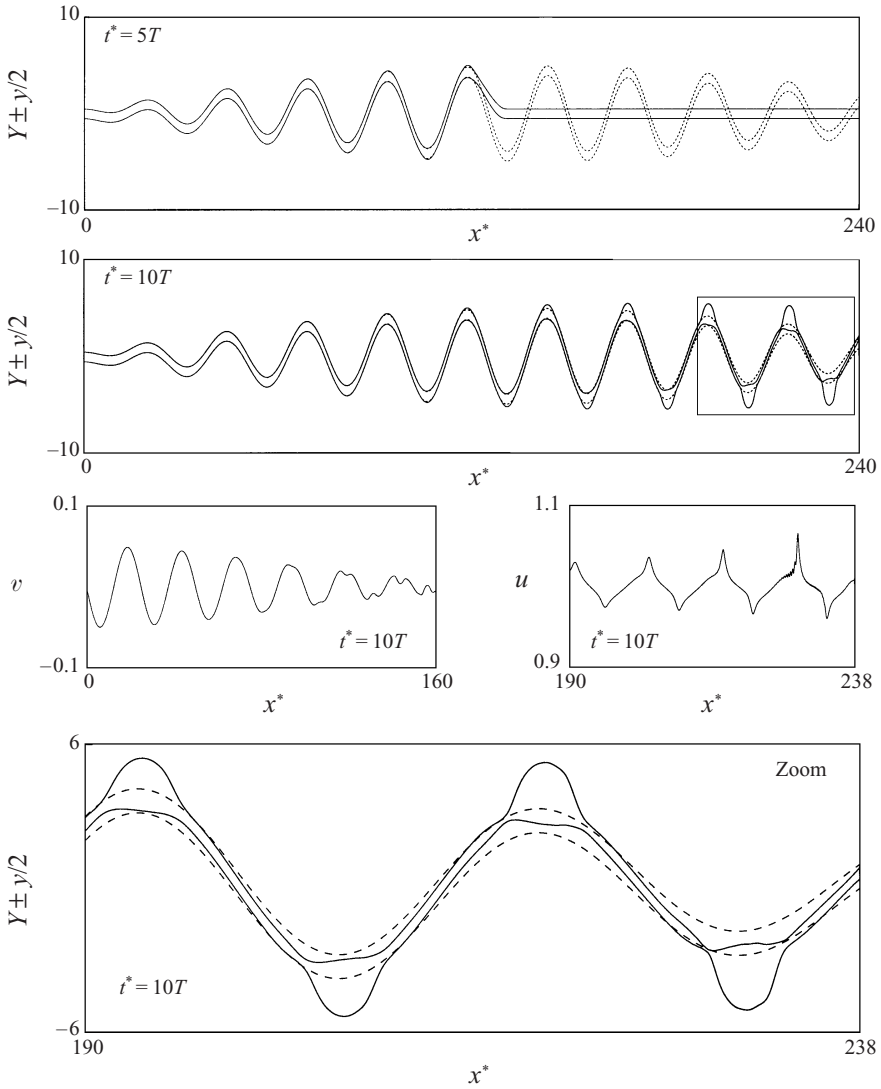

FIGURE 16. Sinuous distortion of a semi-infinite planar liquid sheet harmonically forced at $x^* = 0$ with forcing frequency ω ($A_{Y'} = 0$, $A_{v'} = 0.05$, $We = 1/(2\varepsilon^2) = 1000$, $T = 2\pi/\omega = 25$: – – –, linear limit cycle ($t^* = n\,T$, $n \in$ I); ——, nonlinear transient).

Nonlinear effects similar to those described in the previous paragraph (for fairly large Weber numbers) and as already observed for infinite periodically disturbed sheets were also observed for Weber numbers below the critical value $We_{cr,s} = 2$ (e.g. $We = 1.5$) and a sinuous forcing of the sheet centreline or transverse nozzle location only. (See figure 17.) Note that, as already stated, for $We < 2$ linear theory suggests that only one boundary condition is to be specified at the nozzle exit. Accordingly, the beat behaviour resulting from a superposition of waves with wavenumbers l_1 and l_2, as predicted by linear theory for $We > 2$, is not observed in this case.

Similar to figure 17, figure 18 illustrates the distortion of a liquid sheet with a high surface-tension coefficient of the liquid (i.e. low Weber number). However, in this particular case $We > We_{cr,s}$, i.e. $We = 10$. As in the dilational case shown in figure 13,

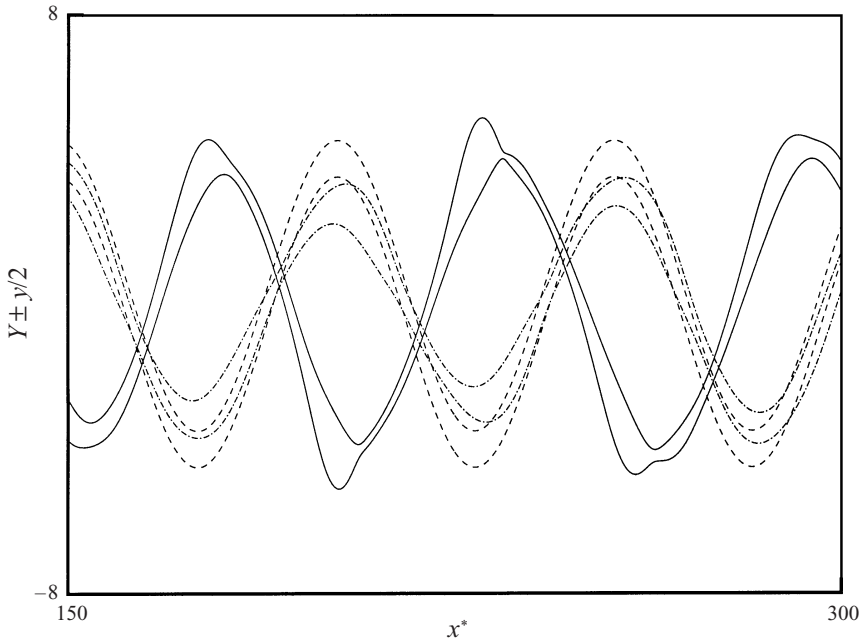

FIGURE 17. Sinuous distortion of semi-infinite planar liquid sheet harmonically forced at $x^* = 0$ with forcing frequency ω ($A_{Y'} = 4$, $We = 1/(2\varepsilon^2) = 1.5 < We_{cr,s}$, $T = 2\pi/\omega = 25$; linear limit cycle: — — —, $t^* = n\,T$ ($n \in \mathrm{I}$); nonlinear transient: — · — ·, $t^* = 12T$; ——, $t^* = 12.7T$).

the momentum disturbance imposed onto the sheet at the nozzle exit is so high that the sheet eventually disintegrates after $t^* > 5T$ and close to the nozzle exit located at $x^* = 0$. However, similarly to figure 14 for dilational disturbances, the characteristic beat behaviour predicted by linear theory is still observed for this highly nonlinear case.

For the various Weber numbers considered above and for small beat amplitudes, linear and nonlinear results agree very well in the disturbed flow regions (not illustrated). An experimental observation of the prescribed beat behaviour was made by Hashimoto & Suzuki (1991) for rather small beat amplitudes on modulated sinuous distorting planar sheets.

5. Conclusions

An unsteady one-dimensional system of equations has been derived governing the nonlinear sinuous (antisymmetric) and/or dilational (symmetric) distortion of thin inviscid planar two-dimensional liquid sheets in a void. The governing equations represent the leading-order equations obtained from the fully two-dimensional problem after series expansion of the dependent flow variables in terms of $[y - \overline{y}(x,t)]$ where y denotes the direction perpendicular to the undisturbed sheet or main flow direction and $\overline{y}(x,t)$ is the instantaneous location of the sheet centreline in the y-direction. Similar governing equations were previously derived and employed by Matsuuchi (1976), Erneux & Davis (1993) and Ramos (1996) for the case of dilational disturbances on infinite sheets only.

For dilational disturbances on infinite sheets, an exact solution for nonlinear periodic travelling waves of constant shape is found similar to those identified by Matsuuchi (1976) and Sirignano & Mehring (1996). The numerical solution using

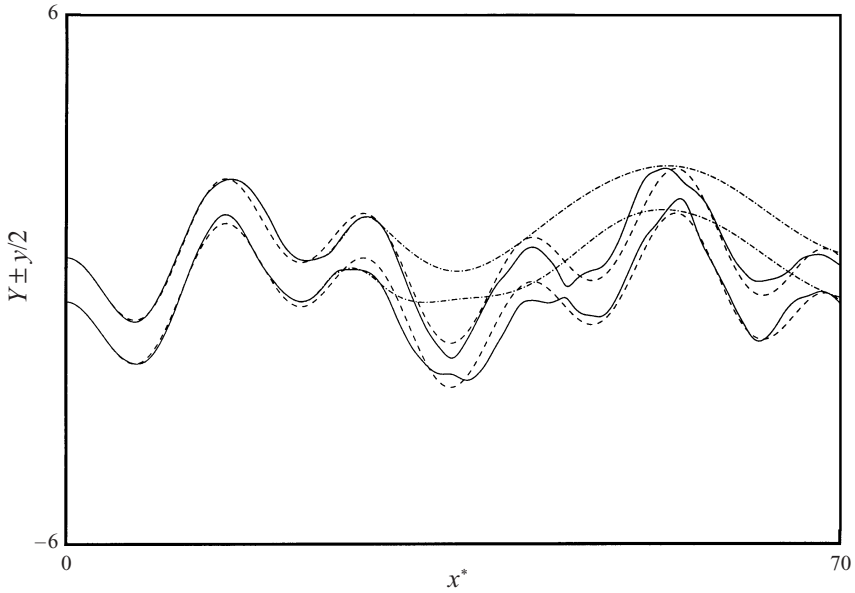

FIGURE 18. Sinuous distortion of semi-infinite planar liquid sheet harmonically forced at $x^* = 0$ with forcing frequency ω ($A_{Y'} = 0$, $A_{v'} = 0.28$, $We = 1/(2\varepsilon^2) = 10$, $T = 2\pi/\omega = 25$; linear limit cycle: — — —, $t^* = nT$ ($n \in$ I); nonlinear transient: — · — ·, $t^* = 2T$; ——, $t^* = 5T$).

the exact waveform for the initial condition maintains constant waveform with time indicating that the exact solution is stable and providing a benchmark for the finite-difference computations. The 'modulational' instability reported by Matsuuchi (1974, 1976) is also identified by nonlinear numerical simulations and for various initial conditions (i.e. wavelength ratios and initial disturbance amplitudes of nonlinear and/or linear travelling waves).

For infinite periodically disturbed sheets, comparison with fully two-dimensional nonlinear simulations shows that the proposed reduced-dimension approach provides representative nonlinear sheet dynamics for both sinuous and dilational disturbances. Both one-dimensional and two-dimensional simulations illustrate that the sinuous and dilational mode of sheet distortion are nonlinearly coupled, resulting in sheet thinning and possibly breakup at each half-wavelength and at points close to the maximum deflection region of infinite sinuous distorting sheets. The nonlinear coupling observed between the sinuous and dilational modes suggests that the 'modulational' instability observed for nonlinear dilational waves might also appear in the superposition of finite-amplitude sinuous waves. The nonlinear one- and two-dimensional simulations also indicate that the sheet distortion, observed for sinuous sheet disturbances in a void and with large disturbance amplitudes, is dominated by the interaction between the first-harmonic dilational and fundamental sinuous modes as suggested by Clark & Dombrowski (1972) with only minor contributions due to higher-harmonic sinuous modes such as those observed by Jazayeri & Li (1996) for the case of an aerodynamically forced sheet. The nonlinear transverse oscillation of sinuous disturbed sheets observed by Rangel & Sirignano (1991) for aerodynamically forced sheets is also observed in the present analysis for an ambient gas of zero density; in the limit of negligible gas density, the results of Rangel & Sirignano (1991) agree with these new results.

In agreement with previous linear one- and two-dimensional analyses of infinite periodically disturbed liquid sheets, the linear analysis of the dimensionally reduced system of equations shows that for thin sheets, i.e. sheets with disturbance wavelengths significantly larger than the sheet thickness, dilational waves are dispersive (with an inverse relationship between wave velocity and wavelength), sinuous waves are non-dispersive and both waveforms are decoupled by linear analysis. The exact nonlinear analysis also demonstrates that dilational waves on thin sheets are dispersive with wave velocity proportional to the reciprocal of wavelength. Due to the dispersive nature of the wave phenomenon, any deviation in the initial nonlinear waveform from the exact solution will result in an unsteady waveform that involves higher harmonics.

Linear and nonlinear analyses of liquid sheets emanating from a nozzle or atomizer with harmonic forcing at the orifice are presented and compared. The simulations show that the nonlinearity does not change some of the character of the sheet distortion identified by the linear analysis; as in the linear case, a sinuous or dilational forcing of the sheet leads (in general) to a sheet distortion characterized by a long-wavelength envelope of a short-wavelength oscillation. However, in the nonlinear case with dilational forcing of the sheet at the nozzle exit, higher harmonics are observed in the unsteady waveform. Also, for nonlinear dilational distorting sheets at high forcing amplitudes of the streamwise velocity component, fluid accumulates into fluid lumps connected by fluid threads, eventually leading to sheet breakup at points close to these fluid blobs.

For a sinuous forcing at the nozzle exit at large Weber numbers or Weber numbers below 2, the nonlinear sheet distortion is similar to the one observed for infinite periodically disturbed sheets, i.e. the sheet takes a sawtooth-like shape with fluid agglomerating in its edges and the possiblity of sheet breakup at points close to the fluid lumps (as in the dilational case) and interspaced by half a wavelength. In none of the observed cases did the nonlinearity lead to continuous steepening of the capillary waves. However, at points of sheet pinch-off, the formation of a singularity in the streamwise velocity component is observed.

For the nonlinear distortion of infinite periodically disturbed thin sheets, the proposed reduced-dimension approach is found to represent accurately the nonlinear sheet dynamics with CPU times that are three orders of magnitude smaller than a fully two-dimensional discrete-vortex-method simulation of the interfacial-flow problem. Furthermore, when compared with an Eulerian method using a VOF/CSF (volume-of-fluid/continuum-surface-force) technique to track the interface location (Kothe & Mjolsness 1992), the reduced-dimension approach provided more accurate solutions to the nonlinear thin sheet problem at significantly shorter CPU times (assuming comparable spatial and temporal resolution in both cases).

The proposed approach is readily extendable to nonlinear analyses of axisymmetric disturbances to thin annular sheets (Mehring & Sirignano 1998*a*, *b*) and to thin conical sheets, and to three-dimensional disturbances to thin planar sheets (Kim & Sirignano 1997, 1998). For the annular axisymmetric case, nonlinear analyses have also been presented by Panchagnula, Sojka & Bajaj (1998) for dilationally distorting sheets only and by Lee & Wang (1988, 1989), the latter for the initial- and boundary-value problem of a collapsing sheet forming a liquid shell. To the knowledge of the authors, a nonlinear analysis of the conical case has not been reported so far. The computational savings by using a reduced-dimension approach will be considerable for these geometrically more complex thin sheet configurations compared to other nonlinear simulations using 'general-purpose' solution techniques designed for interfacial flows of complex topology.

This research has been supported by the US Army Research Office through Grant/Contract No. DAAH 04-96-1-0055 with Dr David Mann as the program manager. Fellowship support for the junior author by the German Academic Exchange Service (DAAD, Doktorandenstipendium HSPII/AUFE) is also appreciated. Dr Inchul Kim was very helpful in applying the finite-difference scheme for infinite sheets and in refining the nonlinear exact solution. Professor Roger Rangel is acknowledged for his contribution to the vortex-dynamics code employed.

REFERENCES

Antoniades, M. G., Godwin, R. & Lin, S. P. 1980 A new method of measuring dynamic surface tension. *J. Colloid Interface Sci.* **77**, 583–585.

Arai, T. & Hashimoto, H. 1985 Behavior of gas-liquid interface on a liquid film jet (Instability of a liquid film jet in a co-current gas stream). *JSME Bull.* **28**, 2652–2659.

Asare, H. R., Takahashi, R. K. & Hoffman, M. A. 1981 Liquid sheet jet experiments: comparison with linear theory. *Trans. ASME: J. Fluids Engng* **103**, 595–604.

Baker, G. R., Meiron, D. I. & Orszag, S. A. 1982 Generalized vortex methods for free-surface flow problems. *J. Fluid Mech.* **123**, 477–501.

Bers, A. 1983 Space-time evolution of plasma instabilities–absolute and convective. In *Handbook of Plasma Physics* (ed. M. N. Rosenbluth & R. Z. Sagdeev), vol. 1, pp. 452–517.

Bogy, D. B. 1978 Wave propagation and instability in a circular semi-infinite liquid jet harmonically forced at the nozzle. *J. Appl. Mech.* **45**, 469–474.

Bogy, D. B. 1979 Drop formation in a circular liquid jet. *Ann. Rev. Fluid Mech.* **11**, 207–228.

Bond, W. N. 1935 Surface tension of a moving water sheet. *Proc. Phys. Soc.* **47**, 549–558.

Boussinesq, M. 1869*a* Théorie des expériences de Savart, sur la forme que prend une veine liquide, après s'être choquée contre un plan circulaire. *C.R. Acad. Sci. Paris* **69**, 45–48.

Boussinesq, M. 1869*b* Théorie des expériences de Savart, sur la forme que prend une veine liquide, après s'être heurtée contre un plan circulaire. *C.R. Acad. Sci. Paris* **69**, 128–131.

Briggs, R. J. 1964 *Electron Stream Interaction with Plasmas.* MIT Press.

Brown, D. R. 1961 A study of the behaviour of a thin sheet of moving liquid. *J. Fluid Mech.* **10**, 297–305.

Clark, C. J. & Dombowski, N. 1972 Aerodynamic instability and disintegration of inviscid liquid sheets. *Proc. R. Soc. Lond.* A **329**, 467–478.

Crapper, G. D. 1957 An exact solution for progressive capillary waves of arbitrary amplitude. *J. Fluid Mech.* **2**, 532–540.

Crapper, G. D. & Dombrowski, N. 1984 A note on the effect of forced disturbances on the stability of thin liquid sheets and on the resulting drop size. *Intl J. Multiphase Flow* **10**, 731–736.

Crapper, G. D., Dombrowski, N. & Jepson, W. P. 1975 Wave growth on thin sheets of non-Newtonian liquids. *Proc. R. Soc. Lond.* A **342**, 225–236.

Crapper, G. D., Dombrowski, N. & Pyott, G. A. D. 1975*a* Large amplitude Kelvin–Helmholtz waves on thin liquid sheets. *Proc. R. Soc. Lond.* A **342**, 209–224.

Crapper, G. D., Dombrowski, N. & Pyott, G. A. D. 1975*b* Kelvin–Helmholtz wave growth on cylindrical sheets. *J. Fluid Mech.* **68**, 497–502.

Dombrowski, N. & Fraser, R. P. 1954 A photographic investigation into the disintegration of liquid sheets. *Phil. Trans. R. Soc. Lond.* A **247**, 101–130.

Dombrowski, N., Hasson, D. & Ward, D. E. 1960 Some aspects on liquid flow through fan spray nozzles. *Chem. Engng Sci.* **12**, 35–50.

Dombrowski N. & Hooper, P. C. 1962 The effect of ambient density on drop formation in sprays. *Chem. Engng Sci.* **17**, 291–305.

Dombrowski, N. & Johns, W. R. 1963 The aerodynamic instability and disintegration of viscous liquid sheets. *Chem. Engng Sci.* **18**, 203–214.

Dombrowski, N. & Munday, G. 1968 'Spray drying'. In *Biochemical and Biological Engineering Science*, chap. 16. Academic Press.

Dorman, R. G. 1952 The atomization of liquid in a flat spray. *Br. J. Appl. Phys.* **3**, 189–192.

Entov, V. M. 1982 On the dynamics of films of viscous and elastoviscous liquids. *Arch. Mech* **34**, 395–407.

Erneux, T. & Davis, S. H. 1993 Nonlinear rupture of free films. *Phys. Fluids* A **5**, 1117–1122.

Ferziger, J. H. 1981 *Numerical Methods for Engineering Application*. John Wiley & Sons.

Fraser, R. P. & Eisenklam, P. 1953 Research into the performance of atomizers of liquids. *Imp. Coll. Chem. Engng Soc. J.* **7**, 52–68.

Fraser, R. P., Eisenklam, P., Dombrowski, N. & Hasson, D. 1962 Drop formation from rapidly moving sheets. *AIChE J.* **8**, 672–680.

Graff, K. F. 1975 *Wave Motion in Elastic Solids*. Dover.

Hagerty, W. W. & Shea, J. F. 1955 A study of the stability of plane fluid sheets. *J. Appl. Mech.* **22**, 509–514.

Hashimoto, H. & Suzuki, T. 1991 Experimental and theoretical study of fine interfacial waves on thin liquid sheet. *JSME Intl J.* II **34**, 277–283.

Heister, S. D. 1997 Boundary element methods for two-fluid free surface flows. *Engng Analysis with Boundary Elements* **19**, 309–317.

Hogan, S. J. 1986 Highest waves, phase speeds and particle trajectories of nonlinear capillary waves on sheets of fluid. *J. Fluid Mech.* **172**, 547–563.

Huerre, P. & Monkewitz, P. A. 1990 Local and global instabilities in spatially developing flows. *Ann. Rev. Fluid Mech.* **22**, 473–537.

Ibrahim, E. A. & Akpan, E. T. 1996 Three-dimensional instability of viscous liquid sheets. *Atomization and Sprays* **6**, 649–665.

Jazayeri, S. A. & Li, X. 1996 Nonlinear breakup of liquid sheets. *Proc. 9th Ann. Conf. Liquid Atom. Spray Sys.*, pp. 114–119. Institute of Liquid Atomization and Spray Systems, North and South America.

Kim, I. & Sirignano, W. A. 1997 Three-dimensional nonlinear temporal stability of infinitely long thin liquid sheets. *Proc. 10th Ann. Conf. Liquid Atom. Spray Sys.*, pp. 132–136. ILASS, North and South America.

Kim, I. & Sirignano, W. A. 1998 Three-dimensional symmetric distortion of thin liquid sheets. *Proc. 11th Ann. Conf. Liquid Atom. Spray Sys.*, pp. 175–179. ILASS, North and South America.

Kinnersley, W. 1976 Exact large amplitude capillary waves on sheets of fluid. *J. Fluid Mech.* **77**, 229–241.

Kothe, D. B. & Mjolsness, R. C. 1992 RIPPLE: A new model for incompressible flows with free surfaces. *AIAA J.* **30**, 2694–2700.

Kothe, D. B., Rider, W. J., Mosso, S. J. & Brock, J. S. 1996 Volume tracking of interfaces having surface tension in two and three dimensions. *AIAA Paper* 96-0859.

Lamb, H. 1932 *Hydrodynamics*, 6th edn. Cambridge University Press.

Lee, C. P. & Wang, T. G. 1988 Dynamics of thin liquid sheets. *Proc. 3rd Intl Colloq. on Drops & Bubbles* (ed. T. G. Wang), pp. 496–504.

Lee, C. P. & Wang, T. G. 1989 The theoretical model for the annular jet instability – Revisited. *Phys. Fluids* A **1**, 967–974.

Lefebvre, A. H. 1989 *Atomization and Sprays*. Hemisphere.

Li, X. 1993 Spatial instability of plane liquid sheets. *Chem. Engng Sci.* **48**, 2973–2981.

Li, X. 1994 Disintegration of viscous liquid sheets. *Proc. 7th Ann. Conf. Liquid Atom. Spray Sys.*, pp. 45–49. ILASS, North and South America.

Li, X. & Tankin, R. S. 1991 On the temporal instability of a two-dimensional viscous liquid sheet. *J. Fluid Mech.* **226**, 425–443.

Lighthill, M. J. 1965 Group velocity. *J. Inst. Maths Applics.* **1**, 1–28.

Lin, S. P. 1981 Stability of a viscous liquid curtain. *J. Fluid Mech.* **104**, 111–118.

Lin, S. P., Lian, Z. W. & Creighton, B. J. 1990 Absolute and convective instability of a liquid sheet. *J. Fluid Mech.* **220**, 673–689.

Lin, S. P. & Roberts, G. 1981 Waves in a viscous liquid curtain. *J. Fluid Mech.* **112**, 443–458.

Mansour, A. & Chigier, N. 1990 Disintegration of liquid sheets. *Phys. Fluids* A **2**, 706–719.

Mansour, A. & Chigier, N. 1991 Dynamic behavior of liquid sheets. *Phys. Fluids* A **3**, 2971–2980.

Matsuuchi, K. 1974 Modulational instability of nonlinear capillary waves on thin liquid sheets. *J. Phys. Soc. Japan* **37**, 1680–1687.

Matsuuchi, K. 1976 Instability of thin liquid sheet and its break-up. *J. Phys. Soc. Japan* **41**, 1410–1416.

Mehring, C., Kim, I. & Sirignano, W. A. 1997 Symmetric distortion of a thin liquid sheet with infinite length. *Proc. 10th Ann. Conf. Liquid Atom. Spray Sys*., pp. 117–121. ILASS, North and South America.

Mehring, C. & Sirignano, W. A. 1997 Symmetric distortion of a thin liquid sheet with semi-infinite length. *Proc. 10th Ann. Conf. Liquid Atom. Spray Sys*., pp. 122–126. ILASS, North and South America.

Mehring, C. & Sirignano, W. A. 1998*a* Nonlinear distortion of infinitely long thin planar and annular liquid sheets. *Proc. 11th Ann. Conf. Liquid Atom. Spray Sys*., pp. 155–159. ILASS, North and South America.

Mehring, C. & Sirignano, W. A. 1998*b* Nonlinear distortion of semi-infinitely long thin planar and annular liquid sheets. *Proc. 11th Ann. Conf. Liquid Atom. Spray Sys*., pp. 160–164. ILASS, North and South America.

Meier, G. E. A., Klöpper, A. & Grabitz, G. 1992 The influence of kinematic waves on jet break down. *Experiments in Fluids* **12**, 173–180.

Meyer, J. & Weihs, D. 1987 Capillary instability of an annular liquid jet. *J. Fluid Mech.* **179**, 531–545.

Nobari, M. R. & Tryggvason, G. 1996 Numerical simulations of three-dimensional drop collisions. *AIAA J.* **34**, 750–755.

Ortner, N. 1978 The initial-boundary value problem of the transverse vibrations of a homogeneous beam clamped at one end and infinitely long in one direction. *Bull. l'Acad. Polonaise des Sci*., Série des Sciences Techniques **26**, no. 8-9, 389–401.

Panchagnula, M. V., Sojka, P. E. & Bajaj A. K. 1998 The non-linear breakup of annular liquid sheets. *Proc. 11th Ann. Conf. Liquid Atom. Spray Sys*., pp. 170–174. ILASS, North and South America.

Pimbley, W. T. 1976 Drop formation from a liquid jet: a linear one-dimensional analysis considered as a boundary value problem. *IBM J. Res. Dev.* **20**, 148–156.

Poo, J. Y. & Ashgriz, N. 1988 Numerical simulation of capillary driven viscous flows in liquid drops and films by an interface reconstruction scheme. *Proc. 3rd Intl Coll. on Drops & Bubbles* (ed. T. G. Wang), pp. 235–245.

Pullin, D. I. 1982 Numerical studies of surface-tension effects in nonlinear Kelvin–Helmholtz and Rayleigh-Taylor instability. *J. Fluid Mech.* **119**, 507–532.

Ramos, J. I. 1992 Annular liquid jets: formulation and steady state analysis. *Z. Angew. Math. Mech.* **72**, no. 11, 565–589.

Ramos, J. I. 1996 Planar liquid sheets at low Reynolds numbers. *Intl J. Num. Meth. Fluids* **22**, 961–978.

Rangel, R. H. & Sirignano, W. A. 1988 Nonlinear growth of Kelvin–Helmholtz instabilities: effect of surface tension and density ratio. *Phys. Fluids* **31**, 1845–1855.

Rangel, R. H. & Sirignano, W. A. 1991 The linear and nonlinear shear instability of a fluid sheet. *Phys. Fluids* A **3**, 2392–2400.

Rayleigh, Lord 1879 On the instability of jets. *Proc. Lond. Math. Soc.* **10**, 4–13.

Richtmyer, R. D. & Morton, K. W. 1967 *Difference Methods for Initial-Value Problems*, 2nd edn. John Wiley & Sons.

Savart, F. 1833 Suite du memoire sur le choc d'une veine liquide lancée contre un plan circulaire. *Ann. Chim. Phys.* **54**, 113–165.

Schlichting, H. & Truckenbrodt, E. 1967 *Aerodynamik des Flugzeuges,* Vol. 1. Springer.

Shen, J. & Li, X. 1996 Instability of an annular viscous liquid jet. *Acta Mechanica* **114**, 167–183.

Shyy, W., Udaykumar, H. S., Rao, M. M. & Smith, R. W. 1996 *Computational Fluid Dynamics with Moving Boundaries*. Taylor & Francis.

Sirignano, W. A. & Mehring, C. 1996 Nonlinear two-dimensional symmetric travelling wave distortion of a thin liquid sheet. In *Dynamics of Exothermicity*, Special Honorific Volume for A. K. Oppenheim. *Combust. Sci. Tech.* Book Series (ed. J. Ray Bowen). Gordon & Breach.

Squire, H. B. 1953 Investigation of the instability of a moving liquid film. *Br. J. Appl. Phys.* **4**, 167–169.

Sussman, M., Fatemi, E., Smereka, P. & Osher, S. 1997 An adaptive levelset method for computing

solutions to incompressible two-phase flows. Presented to the 50th Ann. APS-Meeting/Div. Fluid Mech. *APS Bull. 1997*, Dd9.

Taylor, G. I. 1959*a* The dynamics of thin sheets of fluid, II. Waves on fluid sheets. *Proc. R. Soc. Lond.* A **253**, 296–312.

Taylor, G. I. 1959*b* The dynamics of thin sheets of fluid, III. Disintegration of fluid sheets. *Proc. R. Soc. Lond.* A **253**, 313–321.

Trefethen, L. N. 1984 Instability of difference models for hyperbolic initial boundary value problems. *Comm. Pure Appl. Maths* **37**, 329–367.

Vaynblat, D., Brenner, M., Lister, J. & Witelski, T. 1997 Rupture by van der Waals forces. Presented to the 50th Ann. APS-Meeting/Div. Fluid Mech. *APS Bull. 1997*, Cd2.

Weihs, D. 1978 Stability of thin, radially moving liquid sheets. *J. Fluid Mech.* **87**, 289–298.

Whitham, G. B. 1974 *Linear and Nonlinear Waves*. John Wiley & Sons.

Yarin, A. L. 1993 *Free Liquid Jets and Films: Hydrodynamics and Rheology*. Longman Scientific & Technical.

York, J. L., Stubbs, H. E. & Tek, M. R. 1953 The mechanism of disintegration of liquid sheets. *Trans. ASME* **75**, 1279–1286.

Zak, M. 1979 Dynamics of liquid films and thin jets. *SIAM J. Appl. Maths* **37**, 276–289.